TG–892
MARCH 1967
Copy No. 4

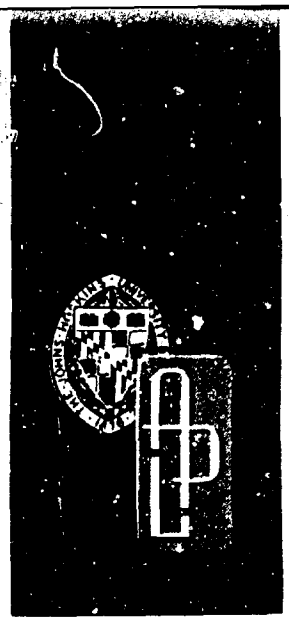

Technical Memorandum

EXTERNAL BURNING RAMJETS PRELIMINARY FEASIBILITY STUDY

by G. L. DUGGER and L. MONCHICK

THE JOHNS HOPKINS UNIVERSITY ▪ APPLIED PHYSICS LABORATORY

93

TG–892
MARCH 1967

Technical Memorandum

EXTERNAL BURNING RAMJETS PRELIMINARY FEASIBILITY STUDY

by G. L. DUGGER and L. MONCHICK

THE JOHNS HOPKINS UNIVERSITY • APPLIED PHYSICS LABORATORY
8621 Georgia Avenue, Silver Spring, Maryland 20910

Operating under Contract NOw 62-0604-c, Bureau of Naval Weapons, Department of the Navy

ABSTRACT

Experiments and analyses at the Applied Physics Laboratory and elsewhere have shown that burning beneath external surfaces of a supersonic vehicle can produce lift and reduce drag. One great advantage of external burning and/or burned gas expansion is that of cooling a greater portion of the engine surfaces by radiation to the atmosphere. This reduction in internal cooling requirements should lead to a weight reduction. A corollary advantage in increased lift-drag ratio is obtained if the burned gas expansion occurs beneath a rearward-facing surface of a two-dimensional or half-round engine.

Preliminary analyses of some two-dimensional external burning ramjet (ERJ) and external expansion ramjet (EERJ) models yield some encouraging results. An analysis suggests that heat addition beneath the rearward-facing surface of a simple inverted triangular section (ERJ) in the form of a normal-plane flame zone stabilized behind a normal shock wave would produce net thrust only when the height of the flame zone exceeds 0.3 or 0.4 of the expansion ramp length. Such a model is of doubtful practicality, however, and does not appear to be representative of burning patterns observed at APL and NASA. A model of greater promise is a compromise between a conventional ramjet and an all-external ramjet which is still designed to permit considerable heat relief for the structure by radiation to the atmosphere, to provide lift, and to provide maximum packaging or fuel storage volume within the engine body. Literally, it is a two-dimensional, external expansion ramjet (EERJ) with a short

subsonic duct (but very little subsonic diffusion) and with critical heat addition at the duct exit serving as the nozzle "throat."

For the EERJ with an ideal, nonreflecting expansion surface, maximum thrust coefficients of 0.26 to 0.90 are calculated for equivalence ratios from 0.25 to 1.0 using kerosene fuel at Mach 5. Fuel specific impulses for high-thrust, low-lift geometries compare with those calculated for a conventional ramjet using similar assumptions on diffuser total pressure recovery (38.3 per cent), combustion efficiency (100 per cent), and nozzle velocity coefficient (0.97 per cent). By varying the cowl-body geometry, a significant lift force can be obtained at the expense of some thrust loss. It appears that the best overall performance will be obtained with a flat-top engine at zero angle of attack with the cowl and effusor geometry designed to turn the burned gas back parallel to the flat top while expanding it to a pressure of approximately three times the ambient pressure. Expansion to lower pressures appears to be neither practical nor desirable. In order to treat a simple case of thrust equals drag for maximum-range cruise, the product of fuel specific impulse and overall lift-drag ratio is estimated for the engine plus added wings for which L/D = 6. A maximum I_f L/D overall of 9000 seconds is estimated for a kerosene-air equivalence ratio of 0.6 at Mach 5. It is estimated that the conventional ramjet plus added wings (wings L/D = 6) would have an I_f L/D approximately 8 percent smaller.

Effects of vectoring the EERJ nozzle and advantages and disadvantages of substituting a simple ramp in place of the non-reflecting surface are explored briefly. The lift and range performance of a simple ramp appears to be always inferior to the maximum values

for an ideal effusor because of appreciable refractions of the characteristics for the Prandtl-Meyer expansion of a real gas along a flat surface.

A comparison of the range versus weight performance of missiles using ramjets, ERJ, or various rockets for second stage propulsion demonstrates the great superiority of the air-breathers, and particularly of an advanced, well-integrated ERJ, in this regard.

A first qualitative consideration of design philosophy for hypersonic transport vehicles incorporating ERJ's for cruise power suggests that there is apt to be a variety of ways in which the ERJ can be integrated with suitable airframes and auxiliary lower speed engines to provide a practical hypersonic aircraft. Three possible paths for the design are pictured and discussed in general terms.

The Johns Hopkins University
APPLIED PHYSICS LABORATORY
Silver Spring, Maryland

TABLE OF CONTENTS

LIST OF ILLUSTRATIONS

LIST OF SYMBOLS

A	area, ft^2
A_e	gas escape area (cowl exit lip to top of engine)
A_F	frontal area of engine (maximum height)
C	force coefficient, force/$q_0 A$
c.g.	center of gravity
c.p.	center of pressure
D	drag force, lb_f (= lb force; lb_m later refers to pounds of mass)
E.R.	equivalence ratio = $f_{actual}/f_{stoichiometric}$
F	force, lb_f
F_g	gross thrust = (exit thrust forces) - (inlet stream thrust) - $P_0(A_e - A_0)$
$\mathcal{F}$	stream thrust $\equiv PA(1 + \gamma M^2)$
f	fuel-air weight ratio
g	gravitational constant, 32.16 ft/sec^2
h	flame height in Section II; specific enthalpy, BTU/lb_m in Sections III and IV
I_f	fuel specific impulse for ramjet or ERJ, $lb_f/(lb_m$ fuel/ sec)
I_{sp}	propellant specific impulse for rocket $lb_f/(lb_m/sec)$
J	mechanical equivalent of heat, 777.5 ft-lb_f/BTU
L	lift force, lb_f
ℓ	expansion ramp length
M	Mach number = $V/\sqrt{\gamma RT}$
P	pressure, lb_f/ft^2

q	dynamic pressure $\equiv \frac{1}{2}\rho V^2$, lb_f/ft^2
R	gas constant, 49706/(molecular weight), ft^2/sec^2-°R, or range, ft, in Sections IV and V
$S°/R$	molar entropy function in Ref. 24, dimensionless
T	temperature, °R
V	velocity, ft/sec
$\dot{w}_a$	air flow rate, lb_m/sec
$\dot{w}_f$	fuel flow rate, lb_m/sec
W_0/W_1	ratio of missile weight at start of cruise to weight at end of cruise
X	mol fraction
α	wedge angle in Section II; angle between flat surface and expansion Mach line in Section IV; ratio of rocket stage metal parts weight to propellant weight in Sec. V.
β	Mach angle $\equiv \sin^{-1} M$
γ	ratio of specific heats, c_p/c_v
δ	flow deflection angle
ρ	density, $\rho = P/RT$, $slugs/ft^3 = (lb/ft^3)/g$
θ	local flow angle. In Section IV, θ_4 = flow angle leaving cowl ≡ wedge angle

Subscripts

0	conditions in free stream
1	conditions after isentropic compression just before normal shock (or after bow shock for Section II)
2	conditions immediately behind normal shock (or after expansion for Section II)
3	conditions in air stream entering constant area section (fuel is added in constant area section between Stations 3 and 4) (or after flame shock for Section II)
4	conditions in burned gas leaving flame, where $M_4 = 1$ (or just ahead of flame for Section II)
5	conditions in expanded burned gas
A	refers to air at Station 3
D	refers to drag force
f	refers to front portion of cowl
F	refers to fuel added between Stations 3 and 4
cl	refers to cowl (or diffuser) lip
g or T	refers to gross thrust of engine
L	refers to lift
n	refers to normal force on surface
i	refers to $i^{\underline{th}}$ pure species
r	refers to rear portion of cowl
t	refers to total or stagnation conditions

THE JOHNS HOPKINS UNIVERSITY
APPLIED PHYSICS LABORATORY
SILVER SPRING MARYLAND

EXTERNAL BURNING RAMJETS
PRELIMINARY FEASIBILITY STUDY*

I. INTRODUCTION

The conventional ramjet engines for the Mach 4 to 5 speed range of these missiles [see Fig. 1(a)] have just about reached the limits of structural design with the more commonly available materials and simple engine cooling techniques such as cooling shrouds or thin interior ceramic coatings. An engine of similar type, that is, with subsonic internal burning and internal exhaust nozzle, designed for appreciably higher flight speeds, Mach 7 to 10 [Fig. 1(b)] would have enormously greater cooling problems. Although the combustion chamber could be much smaller (because the heat release rate would be much larger), the subsonic diffuser would still present a large heat transfer area and the exhaust nozzle length and surface area (supersonic portion) would be much greater because of the larger expansion ratio required. It has been estimated (Ref. 1)[1] that for a Mach 8 engine the cooling requirement imposed by the exhaust nozzle would represent at least half of the total cooling load for the engine, and the small combustion chamber would represent another 15 percent of the total.

An obvious way to reduce the amount of cooling required for such a hypersonic engine by a factor near two, then, would be to use a plug-type, external expansion nozzle. Moreover, if a short combustion zone could be stabilized at the diffuser exit to thermally choke the exit and serve as the nozzle "throat," the cooling problem would be further

---

*This report was originally issued as Confidential CM-948 in 1959. It has been considered of enough general interest to warrant revision to make it Unclassified and to reissue it as TG-892.

[1]References may be found on pp 85-88.

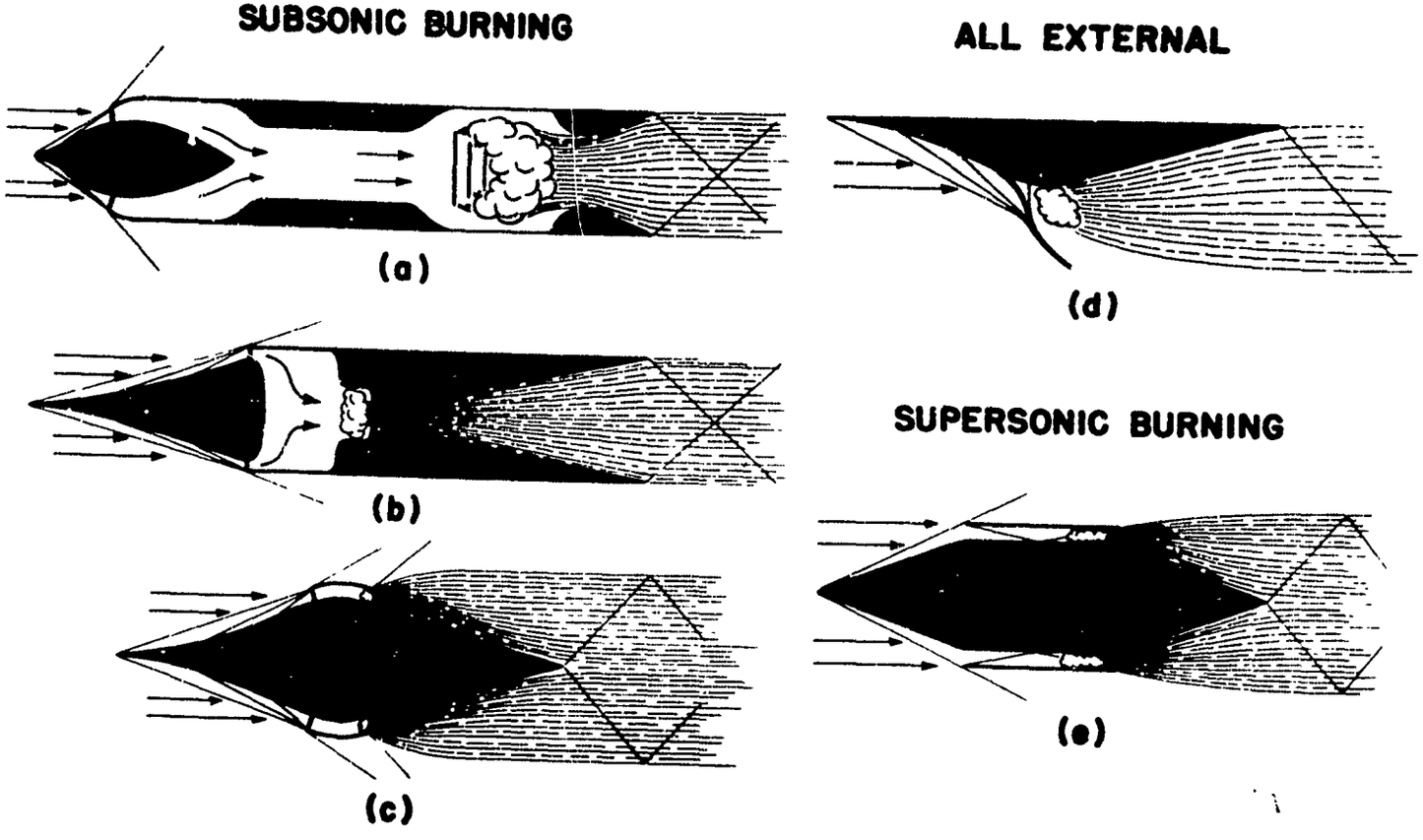

Fig. 1 POSSIBLE PATHS OF EVOLUTION FOR THE HYPERSONIC RAMJET

reduced, because the flame gases and adjacent surfaces could "see" a larger sector of space and of external reradiating nozzle. Such a design [Fig. 1(c)] has been called an "external expansion burning ramjet" or "EERJ." Of course, the ultimate design for making maximum use of cooling by radiation to the atmosphere would be the pure external burning ramjet or ERJ with no ducted flow at all [Fig. 1(d)], but, as will be shown later, it appears much more doubtful that the latter would be practical as a primary power plant with acceleration capability.

Another approach to the hypersonic ramjet engine is, of course, the ducted but supersonic burning concept [see Fig. 1(e)]. The main reason for wanting to keep the flow supersonic throughout is to avoid taking a large shock loss in the diffuser by decelerating the incoming air only to some intermediate supersonic Mach number, say Mach 2 or 3. Analyses (Refs. 2 and 3) suggest that with storable fuels (e.g., kerosene) flight Mach numbers in the range from approximately 5.6 to 10 or even higher should be feasible insofar as calculated net thrust coefficients are concerned. Such a system requires the initiation and completion of combustion in a wholly supersonic gas stream in which the velocity would be of the order of 4000 to 9000 ft/sec. This means that fuel atomization, mixing, and combustion should be completed in a few tenths of a millisecond. Reported experimental work on supersonic burning of storable fuels has been limited to date (Refs. 4 and 5). The possibilities of burning behind a shock wave ("standing wave" or "detonative" ramjet) are also being studied (Refs. 6 through 10) but there have been no reports of engine-type experimental work in this area. Further discussion of these types is considered beyond the scope of this paper. Another potential advantage of the EERJ (relative to a conventional ramjet) arises if one considers the

simultaneous production of thrust and lift. That is, the expansion of burned gases beneath a rearward-facing surface produces a force on that surface which may be resolved into thrust and lift component forces. Proper integration of such an engine into a composite aircraft design might therefore result in a significant increase in lift/drag ratio for the vehicle.

Experimental work at the Lewis Research Center, NASA, produced some very interesting results (Refs. 11 through 14). For example, it was demonstrated that burning aluminum borohydride beneath flat plates and airfoils in a Mach 2.5 stream can produce significant lift forces (enough to double L/D) and that burning around an ogive-cylinder body could reduce drag to practically zero. Linearized flow analyses include those of Gazley (Ref. 15), Mager (Ref. 16), and Willmarth (Ref. 17), all of whom conclude that net thrust should be possible as a result of heat additions to airfoils in supersonic flight. Willmarth also considers the flow field produced by large rates of heat addition near the under surface of a flat plate at M = 2 and concludes that, although for large heating rates (flow deflections of $\sim 20°$) the efficiency drops to approximately half that for the linearized analysis, it is still a respectable efficiency.

To the best of the authors' knowledge, none of the above-mentioned investigators conclusively demonstrated by experiments that positive net thrust could be produced by external burning. The first successful tests in the experimental program at APL were made in March 1959 Aluminum triethyl fuel was burned beneath a simple, all-external, flattop, 10° by 10° wedge model in a 6- by 7-inch Mach 5 tunnel with a stagnation temperature of approximately 1200°F and a

stagnation pressure of 78 lb/in^2 abs. Net thrusts were indicated at small negative angles of attack, with the particular model and, of course, significant lift forces were produced.

The present paper is confined to the preliminary analytical studies which have been made at APL, together with some discussion (contributed by R. H. Cramer) of the integration of two-dimensional ERJ engines into hypersonic airframes.

II. THE ALL-EXTERNAL MODEL OF SMITH AND DAVIS

This section presents a discussion of results obtainable from an all-external model such as proposed by Smith and Davis (Ref. 18), who reasoned that, although the earlier discussions of Pinkel et al., (Ref. 19), Wald (Ref. 20), and others regarding heat additions to supersonic streams were interesting, no practical way of adding heat to supersonic streams was known. They therefore considered the case where heat addition would result in breakdown of the supersonic stream to produce a normal shock. The actual combustion could then be carried out under subsonic flow conditions. Their basic model consisted of a normal shock wave supported by a plane flame front (probably stabilized by a grid flameholder) which was perpendicular to a flat surface of an airfoil.

In the present report, this plane flame and shock system will be considered in relation to the rearward-facing surface of a two-dimensional airfoil having the shape of an inverted isosceles triangle with forward and trailing wedge angle α. The model is sketched in Fig. 2. Undisturbed air approaches through region 0, passes through the oblique bow shock into region 1, undergoes an isentropic Prandtl-Meyer expansion around the hip into region 2, then passes through the normal shock and flame and expands in region 5. Station 3 refers to stream properties immediately downstream of the normal shock and Station 4 to properties just upstream of the flame. The normal shock wave is assumed to remain

APPLIED PHYSICS LABORATORY
THE JOHNS HOPKINS UNIVERSITY
SILVER SPRING MARYLAND

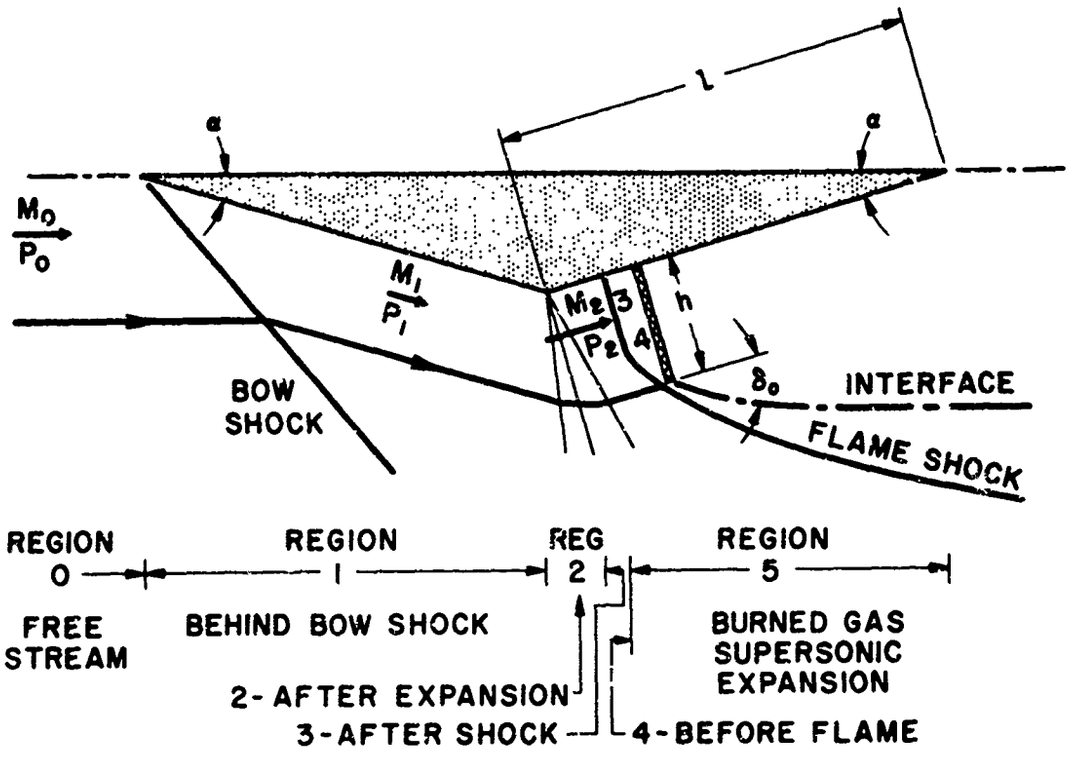

Fig. 2 MODEL OF ALL-EXTERNAL RAMJET WITH NORMAL PLANE FLAME

parallel to the flame front until it intersects the bounding stream line, where it abruptly changes to an oblique shock at the edge of the line flame.

A linearized solution was obtained by Smith and Davis for the normal force on the surface between the shock and the flame which is called F_{3n} herein. (A more sophisticated treatment of the flow in region 3 and 4 has just been done by Woolard (Ref. 21) to be discussed later.) For region 5, the pressure in the burned gas was determined by mass and momentum balances. Immediately downstream of the flame, the pressure in the adjacent air stream is increased to P_5 by the oblique shock which results from its flow deflection through the angle δ by the slip plane. The burned gas is assumed to leave the flame at sonic velocity and to expand supersonically according to the one-dimensional flow approximation (pressure constant along any plane perpendicular to the wedge surface). The nondimensionalized normal forces F_{3n}/P_2h and F_{5n}/P_2h (integrated from excess pressure-distance curves) were given by Smith and Davis for lean and stoichiometric hydrogen flames for M_2's of 2, 3, and 4. In order to find the minimum ratio of flame height to expansion ramp length, h/ℓ, required to produce a positive net thrust on the airfoil, these normal forces have been substituted into the following simple equation (see Fig. 2).

$$F_{net} = P_O \ell \sin\alpha \left[\frac{(F_{3n} + F_{5n})}{P_2 h} \frac{P_2}{P_O \ell} \frac{h}{\ell} - \frac{P_1 - P_2}{P_o} \right] \qquad (1)$$

In Fig. 3, $(h/\ell)_{min}$ has been plotted against flight Mach number M_O (where $M_O < M_2$) for their stoichiometric hydrogen forces. The wedge angle α has been taken as 10°. It appears that h/ℓ should exceed 3/4 even for flight Mach numbers in the range 3 to 5.

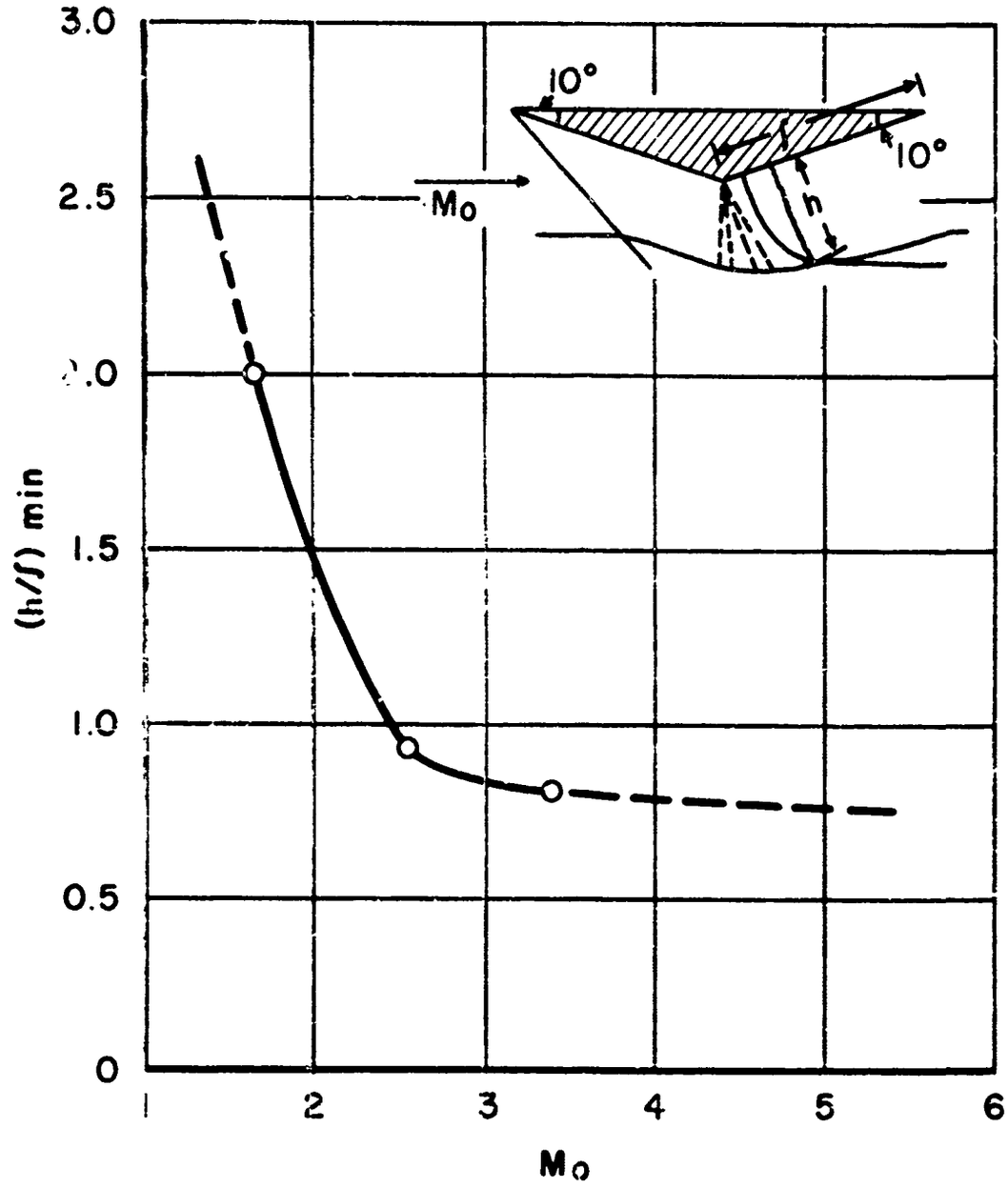

Fig. 3 MINIMUM RATIO OF PLANE FLAME HEIGHT TO EXPANSION RAMP LENGTH REQUIRED FOR NET THRUST

Since the above result does not look very practical, an effort was made to determine the effect of refining the calculation by applying the method of characteristics to the flow behind the flame. For simplicity, the "lean limit" or "critical heat addition" case was studied, in which the separation between shock front and flame is infinitesimal and just enough heat is added to produce sonic velocity at the flame exit plane. The requirement that $M_5 = 1$ is the Chapman-Jouguet condition, so that identification with the well-known model of a detonation wave is complete for this lean limit case. Pressure and direction of burned-gas and adjacent-air flows were equalized by turning the burned gas in a Prandtl-Meyer expansion, letting the expansion waves radiate from the outboard tip of the flame to the wedge. It was found that after a few degrees of expansion, the refraction of these Mach waves by the waves reflected from the surface were slight, so that refraction effects were neglected after $x/h = 1$.

The resultant pressure distribution on the surface behind the flame is shown in Fig. 4 for the case $\gamma = 1.4$, $M_2 = 6.03$. This M_2 corresponds to a flight M_O of 5 for a wedge angle of 10°. A one-dimensional (channel) flow solution for the same conditions is included for comparison. Substitution of the forces determined by the areas under these two curves into Eq. (1) shows that the characteristic solution gives a minimum h/ℓ of 0.42 compared to 1.4 for the channel flow solution. While the former value is much more reasonable than the latter, one still wonders if such a flame height could be practical.

Woolard (Ref. 21) has given a more realistic treatment to this general model, particularly for supercritical heat addition in which the normal shock is detached from the plane flame. Figure 5 is a sketch of the flow pattern with detached shock, which shows that a

APPLIED PHYSICS LABORATORY
THE JOHNS HOPKINS UNIVERSITY
SILVER SPRING MARYLAND

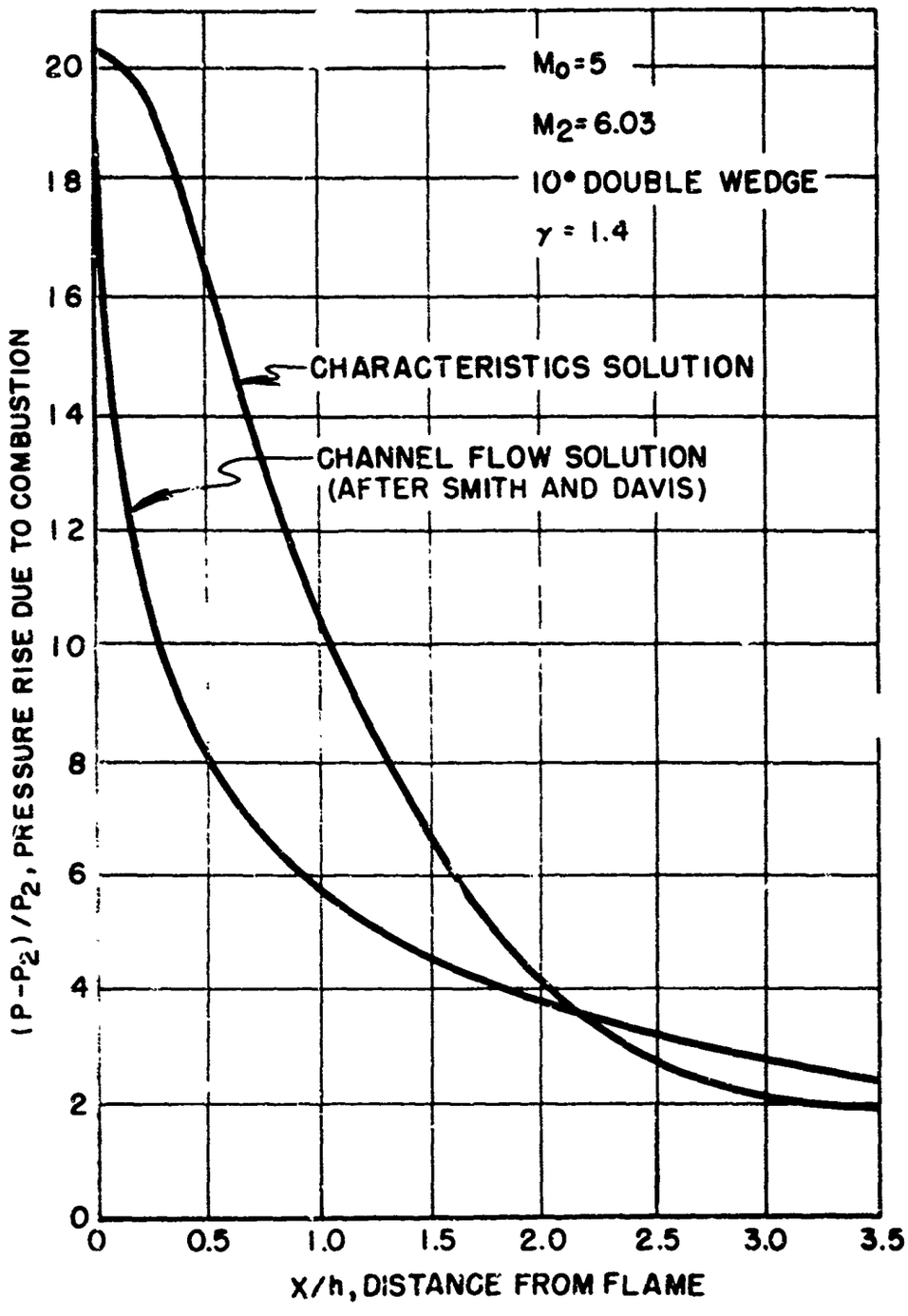

Fig. 4 PRESSURE DISTRIBUTION ON SURFACE BEHIND NORMAL PLANE FLAME CALCULATED BY TWO METHODS

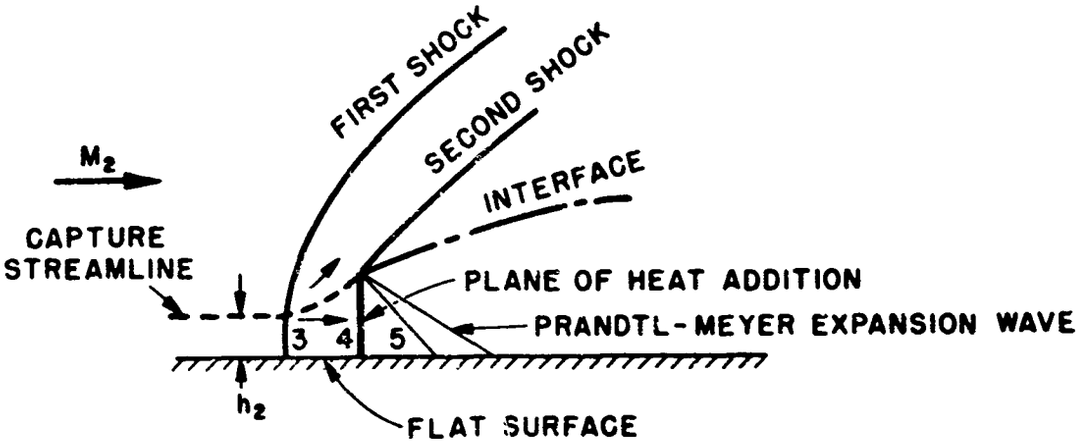

Fig. 5 FLOW CONFIGURATION FOR HEAT ADDITION GREATER THAN CRITICAL WITH NORMAL PLANE FLAME (AFTER WOOLARD)

second shock must emanate from the outboard edge of the heat addition region to serve the purpose of equalizing flow direction and pressure between the spilled air and the burned gases.

For the region between the detached shock and the flame, Woolard calculates normal surface force coefficients approximately four times as great as those given by Smith and Davis, and total after forces, $(F_{3n} + F_{5n})/P_2h$, approximately twice as great. The figures tabulated are based

						Smith and Davis	
M_2	M_4	$\frac{h}{\ell}$	Spillage	$\frac{F_{3n}}{P_2h}$	$\frac{F_{5n}}{P_2h}$	$\frac{F_{3n}}{P_2h}$	$\frac{F_{5n}}{P_2h}$
3	0.266	0.52	0.39	5.0	3.7	1.1	3.1
4	0.321	0.42	0.23	4.8	8.8	1.1	7.2

on Smith and Davis' value for M_4 for stoichiometric hydrogen flames. The h/ℓ values correspond to those required to bring Woolard's C_{5n} to 90 percent of its maximum (expansion to $\ell = \infty$) value; for these h/ℓ's a net thrust would be obtained on a 10° by 10° wedge with Woolard's values, but not with Smith and Davis' (refer to Fig. 3).

The results of Woolard therefore make the pure external ramjet, as represented by this normal plane flame model, a little easier to believe, though the minimum h/ℓ for net thrust would probably still be of the order of 0.3 (no exact correlation between Woolard's results and those previously quoted has been attempted as of this writing). Some fuel distribution system and flameholder extending into the stream would be required to produce and stabilize such a plane flame; these components would add drag and increase the minimum h/ℓ. No way has been

visualized to circumvent the loss caused by the Prandtl-Meyer expansion around the hip or mid-chord of an airfoil--if the flame is on the rear surface, then $M_2 > M_O$, $T_2 < T_O$, $P_2 < P_O$; is the flame is located at or ahead of the mid-chord, the forward normal force now produces drag and the burned gases take the expansion loss so that the after force (behind the flame) is largely dissipated. Thus, one concludes that a reasonable compromise might be to return to the use of a short subsonic duct to capture compressed air and turn it around the hip before adding heat and expanding the burned gases externally.

III. MODIFIED MODEL WITH SHORT COWL (SUBSONIC DUCT) TO TURN COMPRESSED AIR

As noted in the previous section, a serious shortcoming of an all-external model as a thrust-producer is that in order to have the burned gas expansion occur beneath a rearward facing surface, the flow must be turned around a corner or hump in the model. If the flame and its associated shock system are located on the rear surface, this turning requirement causes the incoming air to be accelerated as it goes through a Prandtl-Meyer expansion around the corner, so that the Mach number M_2 approaching the flame shock is actually higher than the free stream or flight Mach number. This high M_2 results in a high total pressure loss through the flame shock system ($P_{t3}/P_{t2} = 0.03$ for Mach 5 flight of the 10° by 10° model). Conversely, if the flame is established just upstream of the knee in the model, then that portion of the burned gas expansion which corresponds to the turning angle around the knee cannot exert any pressure on the rearward-facing surface; moreover any excess pressure on the forward-facing surface caused by combustion contributes to drag rather than thrust.

The external expansion ramjet avoids the flow turning loss. A diagrammatic sketch of the mathematical model is given in Fig. 6. It comprises an external supersonic diffuser, a short cowl and an external or plug-type nozzle, all two-dimensional (or possibly half-round). The approaching air is compressed by the forward isentropic ramp. The rim of the cowl is placed at the point where the inlet is

APPLIED PHYSICS LABORATORY
THE JOHNS HOPKINS UNIVERSITY
SILVER SPRING MARYLAND

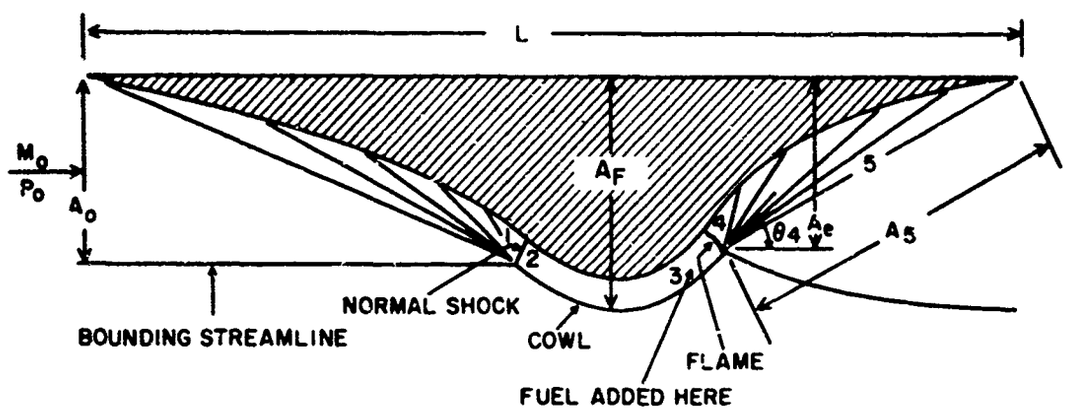

Fig. 6 MODIFIED TWO-DIMENSIONAL ENGINE WITH HIGH-SUBSONIC HEAT ADDITION, "THERMAL THROAT," AND EXTERNAL SUPERSONIC EXPANSION

designed for shock-on rim operation for a given flight Mach number. The functions of the cowl are to capture the appropriate quantity of compressed air, to separate the shock wave and the flame zone so that there is sufficient time for mixing and the ignition lag, and to turn the burned gas to the desired angle θ over the rearward surface so that the supersonic expansion will take the most advantageous pattern with respect to the required thrust and lift production.

In order to stabilize the flame at the cowl exit, the flow under the cowl is expanded or compressed slightly, depending upon the rate of heat addition (fuel-air ratio), which in turn must be just sufficient to accelerate the gases to sonic velocity as they pass through the flame. It is assumed that the required expansion or compression is accomplished between Stations 2 and 3, and that the fuel is added and mixing is accomplished in a constant area duct between Stations 3 and 4. Combustion is completed at Station 4 where $M_4 = 1$.

Preliminary Assessment of Diffuser Variables (Perfect Gas with $\gamma = 1.4$)

Relative effects on thrust of the degree of compression at Station 1 and of subsequent expansion or compression to various M_3's under the cowl (Table I) are estimated with the following simplifying assumptions.

1. All points represent critical operation with shock on rim; for a given M_1, $A_1 = A_2$ = constant, and M_3 is varied by varying A_3.
2. Fuel is injected in a constant area section between Stations 3 and 4 ($A_3 = A_4$) with negligible momentum in the flow direction, so that the momentum balance is

Table I

Preliminary Assessment of Diffuser Variables
for Isentropic Model with Cowl

Perfect Gas, $\gamma = 1.4$. $M_0 = 5$; $T_0 = 393°R$; $P_0 = P_5 = 0.01$ atm $= 21.1$ lb/ft^2;
$T_{t_0} = T_{t_3} = 2360°R$; $\mathcal{F}_0/P_0A_0 = 36.0$; $M_4 = 1$; $\dot{w}_a/P_0A_0 = 0.232$ sec^{-1}; $q_0 = 17.5\ P_0$.

M_1	A_1/A_0	P_2/P_0	M_3	P_3/P_0	P_4/P_0	A_4/A_0	M_5	A_5/A_0	C_T	S_a
2.75	0.133	182.5	0.2	210	90	0.291	4.09	3.39	0.74	278
			0.3	203	95	0.200	4.13	2.41	0.53	197
			0.4	193	98	0.156	4.16	1.93	0.35	160
			0.5	182	102	0.132	4.18	1.67	0.21	140
			0.6	169	108	0.117	4.23	1.53	0.12	128
			0.7	155	109	0.108	4.23	1.41	0.02	121
4.00	0.428	64.4	0.2	71	30.7	0.855	3.31	4.86	0.47	278
			0.3	69	32.3	0.585	3.35	3.45	0.32	197
			0.4	66	33.5	0.461	3.37	2.77	0.19	160
			0.5	62	34.8	0.384	3.40	2.38	0.08	140

$$\mathcal{F}_4 = P_4 A_4 (1 + \gamma_4 M_4^2) = \mathcal{F}_3 = P_3 A_3 (1 + \gamma_3 M_3^2)$$

which reduces to

$$P_4 (1 + \gamma_4) = P_3 (1 + \gamma_3 M_3^2) \qquad (2)$$

3. All gases are ideal gases with a constant specific heat ratio ($\gamma_o = \gamma_3 = \gamma_4 = \gamma_5 = 1.4$).
4. The burned gas undergoes insentropic expansion ($P_{t_5} = P_{t_4}$) from Station 4 (P_4 determined from Eq. (2); $M_4 = 1$) to Station 5, where it is fully expanded to ambient pressure ($P_5 = P_0$; M_5 obtained from resulting P_5/P_{t_5} for $\gamma = 1.4$).
5. The cowl-body geometry is adjusted so that in effect a one-sided isentropic nozzle is provided; that is, the effective slip plane between burned gas and adjacent air stream is parallel to the flight axis, so that the burned gas flow vector at Station 5 is parallel to the flight axis, and $A_5 = A_F$. (A_5/A_4 is calculated from M_5.) (Assumptions 3 and 5 are admittedly naive but are considered adequate to the present purpose; they are corrected in later calculations.)

Thus for selected values of P_O, M_O, M_1, and M_3, the corresponding values of M_5 and A_5 are determined, and the approximate gross thrust is calculated from

$$F_g = \mathcal{F}_5 - \mathcal{F}_O - P_O (A_5 - A_O) \qquad (3)$$

which for convenience is nondimensionalized and re-written in the form

$$F_g/P_OP_O = (A_5/A_O)(1+\gamma M_5^2) - (1+\gamma M_O^2) - [(A_5/A_O) - 1] \quad (4)$$

a thrust coefficient can then be calculated from

$$C_T = \frac{F_g}{q_O A_F} = \frac{F_g}{P_O A_O} \cdot \frac{P_O A_O}{q_O A_5} = \frac{F_g}{P_O A_O} \cdot \frac{2}{\gamma_O M_O^2 (A_5/A_O)}. \quad (5)$$

The results are also related to air specific impulse, S_a, a parameter familiar to jet engineers, which is defined as the critical (M = 1) stream thrust per pound of air per second:

$$S_a = \frac{\mathcal{F}_4}{\dot{w}_a} = \frac{\mathcal{F}_3}{\dot{w}_a} = \frac{P_3 A_3 (1+\gamma_3 M_3^2)}{g\, P_O A_O M_O \sqrt{\gamma_O/R_O T_O}}. \quad (6)$$

Table I gives the results of these over-simplified calculations for a range of M_3's for both $M_1 = 2.75$, which represents a good isentropic ramp diffuser (kinetic energy efficiency of 0.947 for $\gamma = 1.4$), and $M_1 = 4$, which represents a simple 10° wedge. The following general points are shown by this table:

1. For a given M_3 of S_a, the thrust coefficient is increased by 60 percent to 100 percent when M_1 is decreased from 4 to 2.75 by better diffusion.
2. The above statement applies for the range of M_3's of greatest interest, which is shown to be the range of 0.3 to 0.5, because these M_3's correspond to S_a's of 140 to 200, which in turn correspond to the values obtained with common fuels. For example, the complete combustion of kerosene at an equivalence ratio of 0.5, with

air at an inlet total temperature of 2360°F provides an S_a of 160.

3. The above ranges in M_3 and S_a provide a 2-1/2 - fold variation in C_T for the good diffuser ($M_1 = 2.75$). This variation is obtained by a fifty percent change in the nozzle areas A_4 and A_5. These numbers point out the importance of variable geometry at this flight speed, but they also suggest that (as is usually the case for ramjets) higher C_T's might be obtained with smaller A_5's, that is, without full expansion.

Effects of Operational Variables for Fully Expanded Real Gas Cases

Effects of fuel-air equivalence ratio, ambient pressure, flight Mach number, and frozen versus equilibrium exhaust flow were determined for the kerosene-air system (Ref. 22). The air temperatures, pressures, and Mach numbers through Station 3 were calculated as previously except that caloric imperfections were taken into account (Ref. 23). Conditions for the burned gas at Station 4 were determined by mass balance, Eq. (7), momentum balance, Eq. (2), and energy balance, Eq. (8) below, between Stations 3 and 4, allowing for the fuel addition between these two stations and employing the assumption that $V_4 = a_{e_4}$, the sonic velocity under conditions of chemical equilibrium at Station 4. The burned gas was again assumed to expand isentropically to $P_5 = P_O$, and conditions at Station 5 were calculated for both frozen and dynamic equilibrium by entropy and energy balances as follows.

Mass balance:

$$\rho_3 V_3 (1 + f) = \rho_4 V_4 \tag{7}$$

Energy balance

$$\frac{h_{t_A} + f h_{t_F}}{1 + f} = h_{t_4} = h_4 + \frac{V_4^2}{2gJ} = h_{t_5} = h_5 + \frac{V_5^2}{2gJ} , \tag{8}$$

where h_{t_A} and h_{t_F} are the stagnation enthalpies of fuel and air respectively, and other enthalpies are per unit mass of burned gas.

Equations (2), (3), and (8) are satisfied by iteration. One route is to estimate a P_4 (for the present model $P_4 \approx 0.53\ P_2$) then estimate the T_4 and $V_4 = a_{e_4}$ which will satisfy Eq. (8), referring to tables of thermodynamic properties of combustion gases. Now these values of T_4 and V_4 are used to estimate M_3 through $\phi(M_3)$, a tabulated function of Mach number (see Eq. (9) and Ref. 24). This is done by employing Eqs. (2) and (7) together with the perfect gas law and the relationships between Mach number and velocity and between total and static temperature (ignoring, for the moment, caloric imperfections which could cause 0.2 percent error in temperature ratio) to show that

$$\phi(\,) \equiv (1 + \gamma M^2)/[2(\gamma + 1)M^2(1 + \tfrac{\gamma - 1}{2} M^2)]^{1/2} \tag{9}$$

$$\phi(M_3) = (1 + f)\frac{R_4 T_4}{V_4} \frac{(1 + V_4^2/R_4 T_4}{\sqrt{2 \dfrac{\gamma_3 + 1}{\gamma_3} R_3 T_{t_3}}}$$

from which it is seen that $\emptyset(M_3)$ is primarily dependent on T_4, V_4, and $T_{t_3} = T_{t_0}$, because appropriate values of γ_3 and R_4 will fall within narrow ranges. Knowing $\emptyset(M_3)$ from Eq. (9a) one could then solve for M_3 from Eq. (5) or by interpolation for $7/5 < \gamma_3 < 9/7$ in the tables of Ref. 24.

The pressure P_3 and area $A_3 = A_4$ may be obtained from normal shock tables, corrected for caloric imperfections; P_4 is then recalculated from the momentum balance and compared with the assumed value. The process is iterated until the difference between estimated and recalculated P_4 is too small to noticeably affect V_4 and the corresponding h_4.

Exit conditions at station 5 were then obtained by energy (Eq. 8) and entropy balances. For dynamic equilibrium, in which the chemical composition is allowed to shift with T and P, the properties of the burned gas may be read directly from the tables of Ref. 22 by interpolating to $s_5 = s_4$ at the exit pressure $P_5 = P_0$. The energy balance then gives V_5, and the mass balance between stations 4 and 5 gives A_5. The stream thrust at station 5 is then calculated from

$$\mathcal{F}_5 = P_5 A_5 (1 + V_5^2/R_5 T_5) \tag{10}$$

and gross thrust is calculated from Eq. (3).

For frozen equilibrium, where the burned gas composition (mol fractions, mean molecular weight) at station 4 is assumed to hold for all points further downstream, the equation for the isentropic process is

$$\sum_i X_{i_4} (S^\circ/R)_{i_4} - \ln(P_4/P_5) = \sum_i X_{i_4} (S^\circ/R)_{i_5} \tag{11}$$

where the mol fraction and entropy function for each pure product species is obtained from the tables at T_4, P_4. The T_5 which satisfies this equation at $P_5 = P_O$ is found by trial and error from interpolation in the tables. The specific enthalpies of the various product species at this temperature are then used to calculate the burned gas specific enthalpy, which is next used in the energy equation to calculate V_5; $R_5 = R_4$.

Results of these calculations are presented in Table II. Points to be noted are

1. Thrust coefficients are encouragingly high and far outweigh the major engine drag force, the cowl lip drag, which is crudely estimated at the bottom of the table.
2. As one might expect, fuel economy as represented by fuel specific impulse [lb gross thrust/(lb-fuel/sec)], decreases slightly as fuel-air equivalence ratio is increased from 0.25 to 0.70.
3. There is little difference between frozen and dynamic equilibrium results at Mach 5. (Only the E.R. = 0.7 results are shown in the table, but there was even less difference at lower equivalence ratios as one might expect.)
4. Effect of altitude in the isothermal range will be negligible.
5. Thrust coefficient and fuel specific impulse fall off rapidly as flight Mach number approaches 8. Since drag would decrease only very slightly as speed increased, a zero net thrust condition would soon be reached at E.R. = 0.5. Note, however, that the overall efficiency of the engine, as represented by the product of velocity and fuel

Table II

Fully Expanded Operation of Isentropic ERJ with Cowl Effects of Flight Speed, Pressure, Fuel-Air Ratio, and Chemical Equilibria
Real Gas, Kerosene-Air

Engine	ERJ							RJ
Free stream								
M_0	5				5	6	8	5
P_0, atm	0.1				0.10	0.01	0.01	0.01
T_0, °R	2220				20	2950	4740	2220
Normal Shock								
M_1	2.75				2.75	3.25	4.10	2.75
V_1/V_2	0.1293				0.1293	0.0959	0.0499	0.1293
P_2/P_1	0.483				0.483	0.447	0.325	0.483
Fuel Equiv. Ratio	0.25	0.50	0.70	1.0	0.50	0.50	.50	0.50
Isentropic Diff.								
M_3	0.488	0.393	0.351	0.346	0.392	0.445	0.561	0.644
P_3, atm	1.919	2.021	2.060	2.066	20.02	3.920	11.10	2.236
T_3, °R	2135	2167	2175	2180	2.[illegible]	2860	4525	2219
A_3/A_4	0.1283	0.1519	0.1670	0.1694	0.152	0.096	0.032	1.250
Throat, M_4 = 1*								
V_4, fps	2488	2761	2907	3012	2733	2926	3240	2765
P_4, atm	1.100	1.082	1.087	1.112	10.79	2.218	7.13	1.234
T_4, °R	2786	3542	4058	4469	3555	4059	5107	3551
Exit								
Chem. Comp.**	D	D	F	D	D	D	D	D	D
V_5, fps	5760	6580	7033	7120	7765	6570	7370	8840	6410
T_5, °R	862	1201	1428	1485	1920	1204	1200	1291	1425
A_5/A_F	1.877	2.320	2.640	2.698	2.040	2.337	2.490	2.900	1.250
F_5/P_0A_0	43.98	51.22	55.84	56.35	58.54	51.17	68.07	107.9	50.24
Performance								
$C_T = F_g/q_0A_F$	0.216	0.342	0.394	0.395	0.385	0.338	0.242	0.119	0.639
$I_f = F_g/\dot{w}_f$	1810	1780	1660	1700	1310	1770	1620	1240	1790
Drag, $C_{D_{10°lip}}$***	0.053	0.065	0.072	0.072	0.077	0.066	0.064	0.062	0.023

*Stagnation specific enthalpy of air = 565 Btu/lb at 2220°R, fuel assumed to enter at 177°F with 489 Btu/lb.

** F - Composition frozen beyond station 4. D = composition shifting with T and P in dynamic equil.

***Wave drag of 10° cowl lip on projected area $A_F - A_0$.

specific impulse increases with Mach number (it may pass through a maximum between 6 and 8).

6. Comparison of the last column for a ducted ramjet with the second column for the ERJ, both with the same assumptions on diffuser total pressure recovery (39.4 percent) and combustion efficiency (100 percent), shows that the ERJ, if it could in fact obtain full isentropic expansion, would produce comparable I_f, but would have a much lower C_T and higher C_D because of its large frontal area. The arbitrarily chosen area ratios for the ramjet, which are typical of current practice, result in underexpansion. Subsequent calculations will show that the ERJ also benefits from a reduction in drag at the penalty of underexpansion.

Effects of Cowl-Body Geometry, Varying Expansion Real Gas Cases

A few cases of underexpansion were solved to obtain a feeling for the balance between the effects of cowl drag and degree of expansion on the gross thrust and lift of the system. The method of characteristics was used to obtain the pressure distribution on the surface aft of the cowl.

The same assumptions regarding the approach flow and plane flame zone are made, so that the conditions at station 4, immediately downstream of the flame front, are the same as those given in Table II for $M_O = 5$, $P_O = 0.01$ atmosphere, and the appropriate equivalence ratio. For simplicity, it is assumed that the after surface is an isentropic surface and that Prandtl-Meyer expansion occurs from the cowl lip. For a given A_e/A_O, the ratio of cowl escape area to capture area,

and a given flow angle θ_4 on the downstream side of the flame, the parameters required to calculate the forces at the last Mach line to hit the missile are determined as follows. The pressure and temperature at any Mach line are determined as functions of V by energy and entropy balances, assuming dynamic equilibrium in the burned gas (see Eq. (8) and previous discussion on dynamic equilibrium). From the tables of properties of combustion gases, the acoustic velocity a, and hence the Mach angle, $\beta = \sin^{-1} a/V$, may be determined as a function of V. The local flow angle θ is then determined from

$$\theta = \theta_4 - \int_{a_4}^{V} \cot\beta \frac{dV}{V} . \qquad (12)$$

The area A_5, represented by the length of the last Mach line, is determined by mass balance

$$A_5 \rho_5 V_5 \sin\beta_5 = \rho_4 V_4 A_4 . \qquad (13)$$

A_e is related to A_5 by

$$A_e = A_5 \sin(\theta_5 + \beta_5) . \qquad (14)$$

The stream thrust across the last Mach line is

$$\mathcal{F}_5 = P_5 A_e + (P_5 A_5 V_5 \sin\beta_5 / R_5 T_5)(V_5 \cos\theta_5) . \qquad (15)$$

These relationships may be seen from Fig. 7.

Using this $\mathcal{F}_5$, thrust coefficient and fuel specific impulse are calculated as before. Lift forces are calculated for the same force

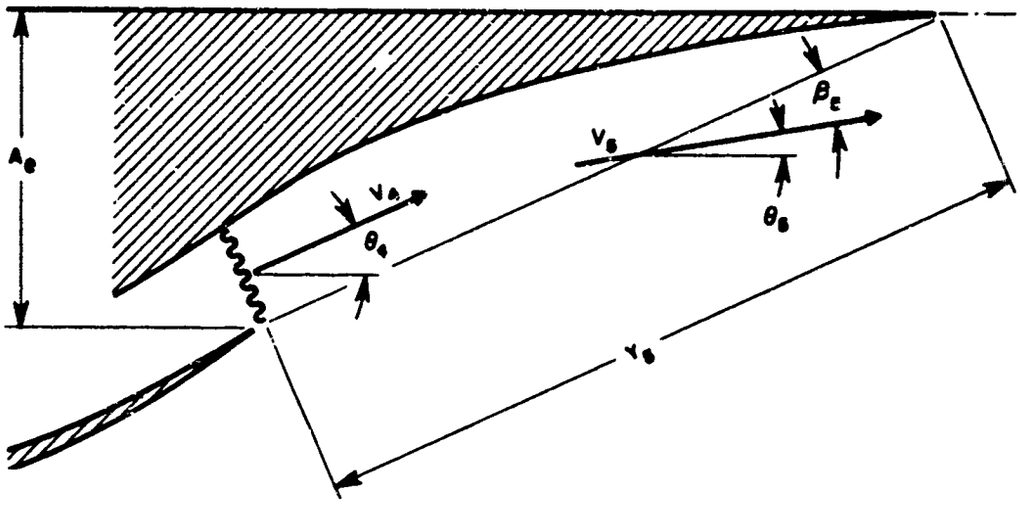

Fig. 7 MODEL FOR CALCULATION OF EXIT FORCES AT LAST MACH LINE STRIKING NONREFLECTING EFFUSOR SURFACE

envelope used in the thrust calculation. Since the bounding streamline between stations 0 and 1 is parallel to the flight axis and undisturbed, no momentum is transported across it, and the pressure force on it is equal and opposite to the pressure force on the corresponding portion of the flat top missile surface. Hence the left forces need be evaluated only for the last Mach line, the cowl, and the corresponding areas on the top surface.

$$L_{5_{net}} = (P_5 - P_O) A_5 \cos(\theta_5 + \beta_5) + (P_5 A_5 V_5 \sin\beta_5 / R_5 T_5) \cdot (V_5 \sin\theta_5), \quad (16)$$

$$L_{c_{net}} = L_c - P_O A_c , \quad (17)$$

where A_c is the longitudinal projected area of the cowl, and

$$C_L = (L_{5_{net}} + L_{c_{net}})/q_0 A_F . \tag{13}$$

(Further details for the calculation of L_c are given in Appendix I.)

For any chosen θ_4 (flow angle leaving the cowl) and A_e/A_0 (ratio of cowl escape area to capture area), one can calculate C_T and I_f from the gross thrust and C_L from Eq. (18). For example, one can choose a θ_4, say, one radian, and vary A_e/A_O to obtain curves of the above parameters versus A_e/A_o. As A_e/A_O is increased, one will approach the point in the calculations where the last Mach line to strike the missile will have turned the flow parallel to the flight axis; that is, the velocity vector $\vec{V}_5$ will be parallel to the flight axis and θ_5 will be zero. Further isentropic expansion without reflection of Mach lines would require the expansion surface to turn away from the flight axis again, a case which would probably not be desirable in the overall missile design. (It would result in decreased thrust and increased drag and would perhaps make the engine more difficult to integrate with an airframe; it would, however, provide more lift, but a flat plate extension would also accomplish this without the thrust penalty.) At any rate, it was decided to terminate these calculations at $\theta_5 = 0$.[2]

Figure 8 illustrates the general configurations of the sets of curves which can be developed in this manner and the way that they are

[2] One might ask whether it is valid to carry these calculations for a Prandtl-Meyer expansion even to the point $\theta_5 = 0$. Examples in Appendix II show that, at least in the region of greatest interest, this procedure is valid.

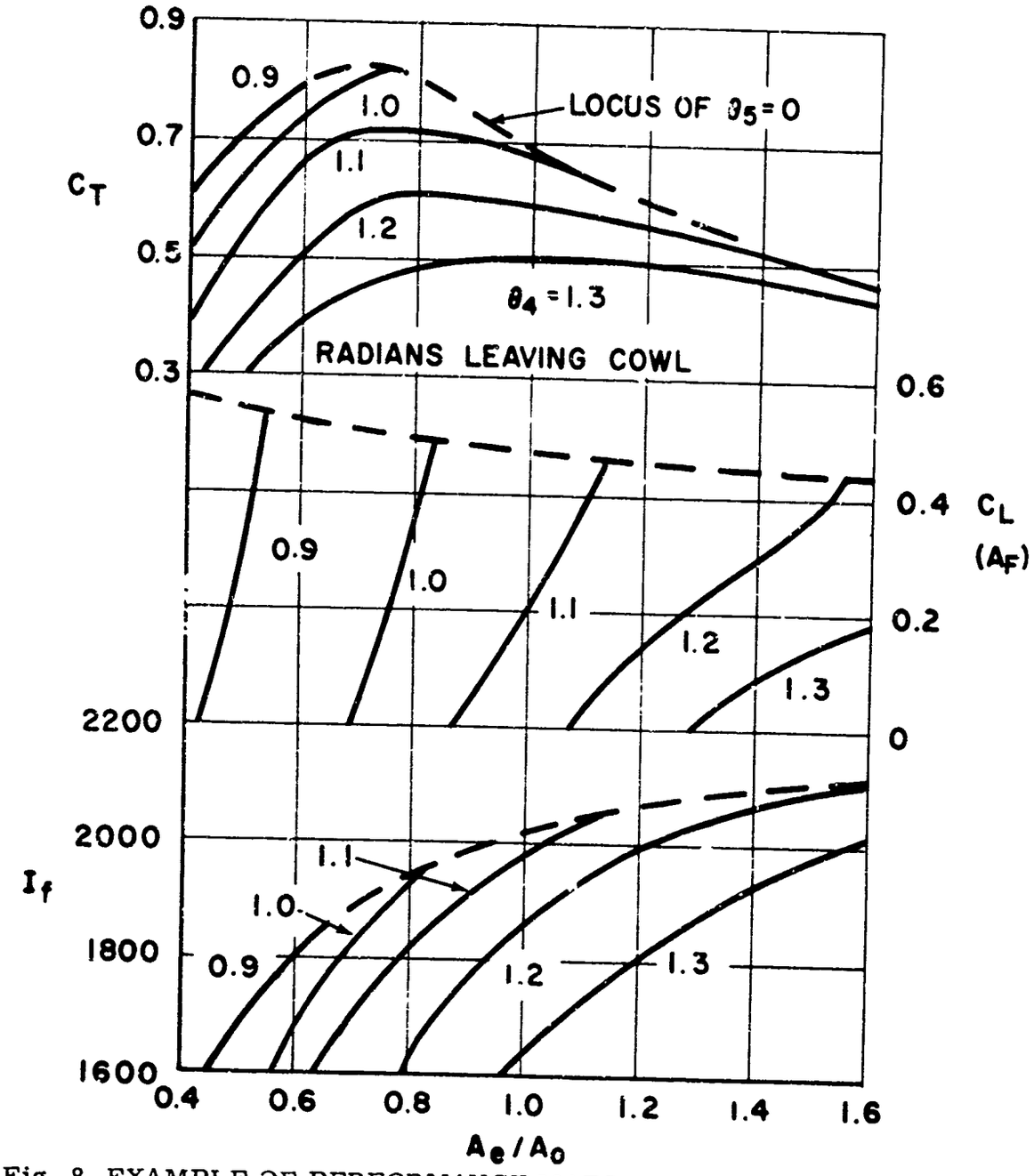

Fig. 8 EXAMPLE OF PERFORMANCE MAPS FOR LERJ PRODUCED BY VARYING A_e/A_0 AT VARIOUS θ_4's

Curves are terminated at $\theta_5 = 0$, which is considered the limit of practical interest. Numerical values are not comparable to subsequent figures because they are incorrectly based on a_f.

terminated at the "locus of $\theta_5 = 0$." This figure is presented here for two reasons: to illustrate the shapes of the curves, and to point out the considerable errors which can be introduced into such calculations by the use of improper acoustic velocities. In calculating the curves for Fig. 8, it was assumed that the burned gases were in dynamic equilibrium; however, it was erroneously assumed that since a characteristic (Mach wave) represents an infinitely thin mathematical surface, there would be no time for chemical change in crossing it and the frozen sonic velocity should be used even in dynamic equilibrium calculations. This is not correct, because in the basic potential flow equation from which differential equations are obtained for the characteristics, the local value of a is used, and this value is determined by the thermodynamic nature of the gas, that is, $a = dp/d\rho$. Therefore in dynamic equilibrium calculations one should use the equilibrium acoustic velocity a_e rather than the "frozen" acoustic velocity a_f.

The numerical values of Fig. 8 should not be used by the reader for any further purpose, because the C_T and I_f values are erroneously high, whereas the lift coefficients are low.

Rather than recalculate all of the curves generated for figures such as Fig. 8, it was decided that an investigation in greater detail be made of the more interesting but restricted case which represents the maxima in various parameters for isentropic expansion without wall reflections, namely, the case of $\theta_5 = 0$, using the correct equilibrium sound velocity. This was done by setting $\theta = \theta_5 = 0$ in Eq. (12) so that for each θ_4 there is a corresponding value of the local velocity which will have been reached when the flow has become parallel to the flight axis (or flat top of the engine).

The basic parameter being investigated in this case is the degree of underexpansion, that is, the ratio P_5/P_O at the point where $\theta_5 = 0$. In other words, the cowl-body geometry is varied to produce various degrees of underexpansion, but in all cases it is assumed that the geometry is designed to give the maximum ($\theta_5 = 0$) value of the performance parameter corresponding to that P_5/P_O. The first figure in this series, Fig. 9, therefore presents the relationships between P_5/P_O and the geometry variables, θ_4 and A_e/A_O, required to produce $\theta_5 = 0$ at various kerosene-air equivalence ratios for a flight speed of Mach 5 and P_O = 0.01 atmosphere and $T_O = 395°R$. The results are thereafter presented as functions of P_5/P_O and are discussed in the following section.

Discussion of Results for Varying Expansion, Real Gas

Figure 10 presents the thrust coefficients for various cases as functions of the degree of underexpansion, P_5/P_O, with geometry adjusted to give $\theta_5 = 0$, as discussed in the previous section. All of the calculations assume 100 percent combustion efficiency. The uppermost curve in Fig. 10 also assumes a nozzle velocity coefficient of unity (no losses in expansion). All other curves in this and subsequent figures are based on a nozzle velocity coefficient C_V of 0.97. Here it is assumed that any deficiency in mass flow which would have resulted with a theoretical nozzle (boundary layer effects) has been compensated in the nozzle design, so that the 0.97 coefficient applies only as a first power effect on velocity V_5.

Effect of Nozzle Velocity Coefficient on C_T

The difference between the first and second uppermost curves of Fig. 10 indicates the effect of a 3 percent loss in exit velocity when

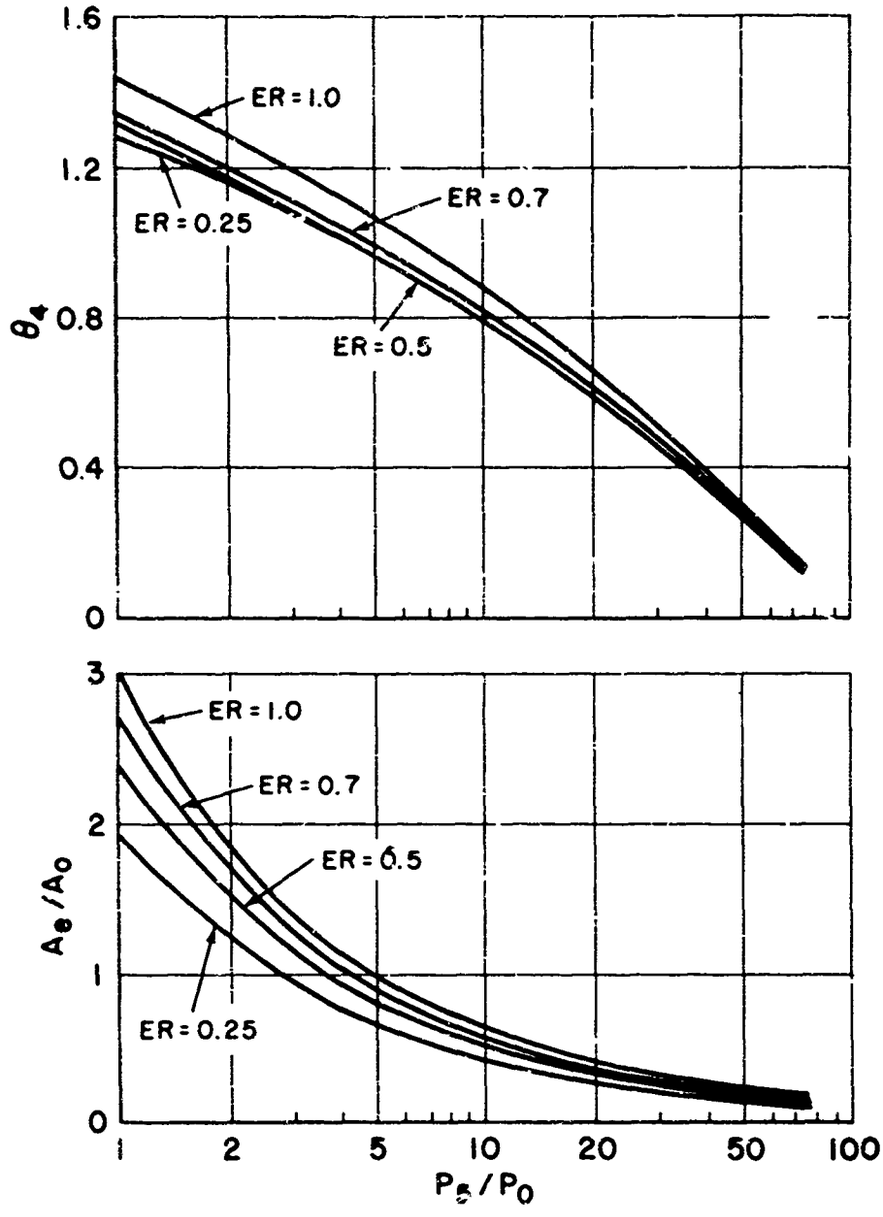

Fig. 9 INDEX CURVES FOR $\theta_5 = 0$ CALCULATIONS OF FIGS. 10 THROUGH 15; RELATIONSHIPS BETWEEN θ_4, A_e/A_0, AND P_5/P_0 FOR VARIOUS KEROSENE-AIR EQUIVALENCE RATIOS

Real gas; dynamic equilibrium; $P_{t_2}/P_{t_0} = 0.383$; $\eta_c = 1.00$; nonreflected Prandtl-Meyer expansion, based on equilibrium sound velocity a_e.

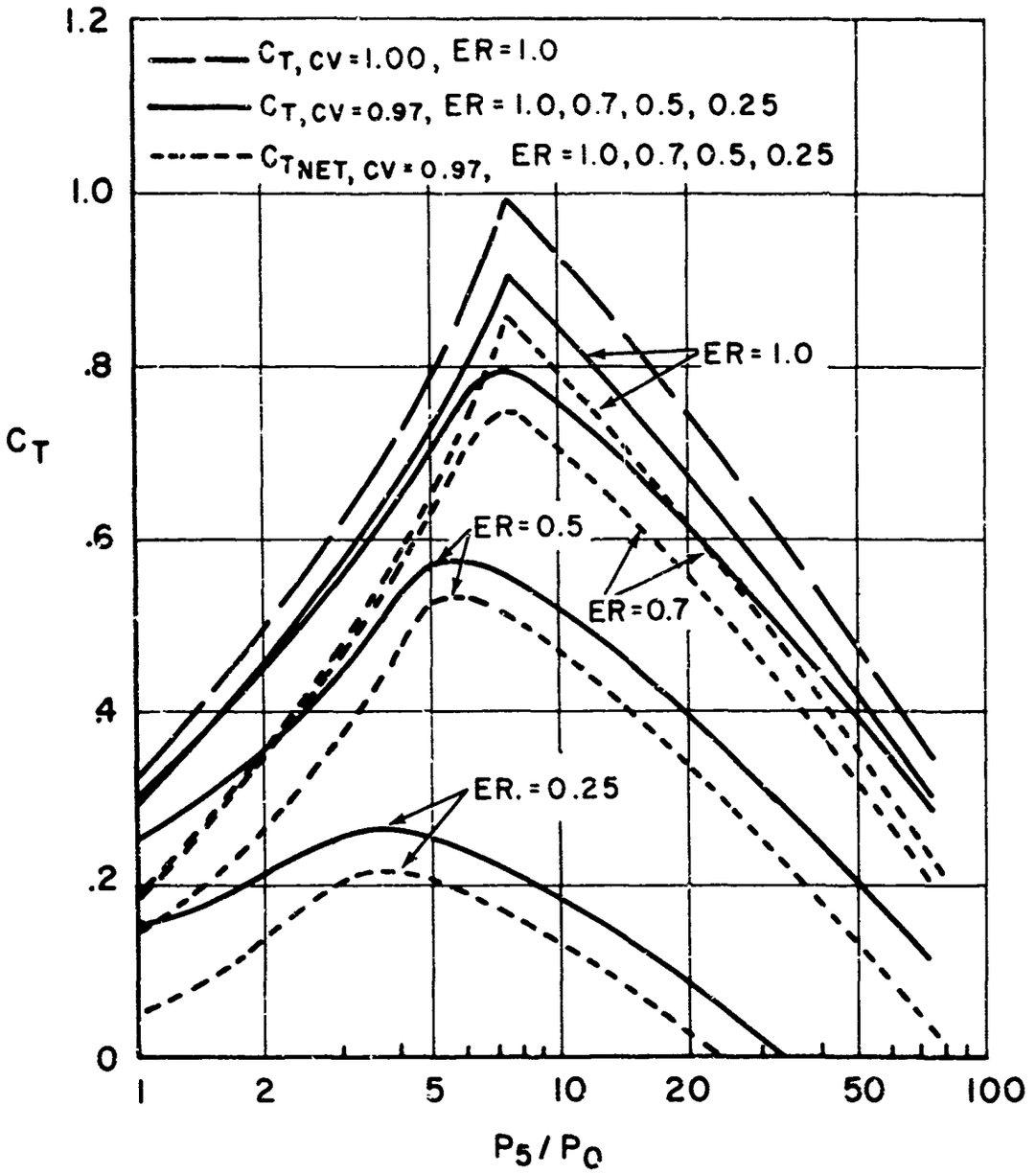

Fig. 10 THRUST COEFFICIENTS VERSUS EXPANSION RATIO, P_5/P_0, FOR MODIFIED ENGINE WITH $\theta_5 = 0$, AT VARIOUS EQUIVALENCE RATIOS

Upper curve for E. R. = 1.0 based on nozzle velocity coefficient $C_V = 1.00$; solid curves based on $C_V = 0.97$ (see text); dashed curves represent net thrust coefficient ($C_V = 0.97$) after subtracting estimated drag. Other assumptions are the same as in Fig. 9.

burning kerosene at an E.R. of 1.0. The thrust loss is approximately 9 percent. Each point lost in C_V therefore results in a 3 percent loss in thrust at E.R. = 1.0, and could result in as much as 6 percent loss at this equivalence ratio if the geometry were not corrected for boundary layer effects or were operated off-design (for example, by simply adjusting the cowl over a body that was designed for different operating conditions). At lower equivalence ratios the effect of C_V on C_T is even greater, because the difference between exit stream thrust and the fixed entrance stream thrust decreases with equivalence ratio, so that a given loss in exit stream thrust is magnified in its effect on gross thrust and thrust coefficient. For example, at E.R. = 0.25 each point lost in C_V would cause a 6 percent loss in maximum C_T (with a mass-flow compensated geometry).

Effe . of Underexpansion on C_T

All of the curves of Fig 10 illustrate that better thrust coefficients (based on required engine frontal area) are indeed obtained when the burned gas is underexpanded as it leaves the isentropic expansion surface. For the richer mixtures, E.R. = 0.7 to 1.0, the thrust coefficients peak rather sharply at an exit-to-ambient pressure ratio of seven to eight. For lower P_5/P_O, the frontal area A_F must be increased in order to provide the A_e/A_O corresponding to the flow turning angle θ_4 which is necessary to reach that P_5/P_O; since A_F increases more rapidly than the gross thrust (with the present assumptions on geometry, Appendix I) C_T based on frontal area decreases.

At lower equivalence ratios, the peak occurs at lower P_5/P_O, but even at E.R. = 0.25, which is probably near the practical lower limit with regard to gross thrust fuel economy (Fig. 11), a pressure ratio $P_5/P_O = 3$ should be maintained.

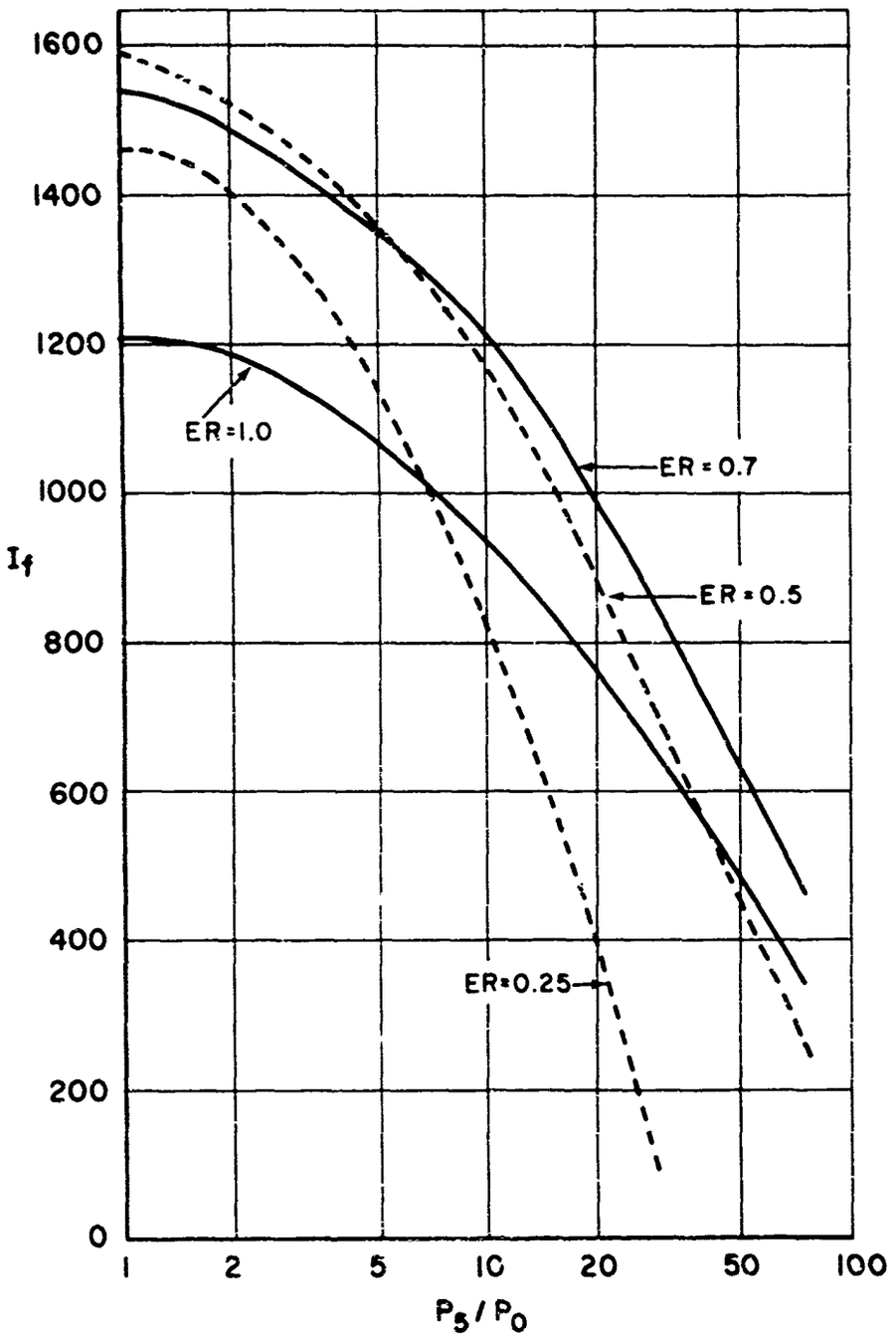

Fig. 11 FUEL SPECIFIC IMPULSE VERSUS P_5/P_0 FOR VARIOUS EQUIVALENCE RATIOS BASED ON C_T FROM FIG. 10

Effect of Equivalence Ratio on C_T

The solid curves of Fig. 10 compare C_T's with $C_V = 0.97$, for equivalence ratios of 1.0, 0.7, 0.5, and 0.25. Maximum C_T is roughly proportional (and early equal to) equivalence ratios in the range of 0.25 to 0.7, but increases more slowly from 0.7 to 1.0 and probably falls off beyond E.R. = 1.0. The latter effect is more pronounced on either side of the optimum expansion ratio, that is the E.R. = 0.7 and E.R. = 1.0 curves converge for either high or low expansion.

Effect of Engine Drag

The difference between the solid curve and the dashed curve for each equivalence ratio in Fig. 10 represents the estimated engine drag coefficient. (See Appendix I for method of estimation.) Pressure ratios of 5 to 50 represent short engines with relatively low friction drag and cowl pressure drag, so that the estimated engine drag coefficients fall in the range 0.05 to 0.07. For greater or lesser expansion, $P_5/P_O < 5$ or < 50, the engine must be lengthened, and the estimated drag coefficients increase to 0.09 to 0.11. Moreover the latter values probably should be even higher, because the geometry assumptions lead to a long subsonic duct for either very large or very small A_e/A_O (Fig. 9), and no allowance was made in these drag estimates for internal friction losses.

Fuel Specific Impulse

It is not surprising that the maximum I_f (defined as gross thrust per pound of fuel burned per second, $I_f = F_g/\dot{w}_f$) is obtained with complete expansion in all cases. Figure 11 indicates that the best fuel economy for this engine, burning kerosene, will occur with an equivalence ratio between 0.5 and 0.7. At maximum C_T conditions, with

E.R. $\sim$ 0.6 and $P_5/P_O \sim 7$, a maximum practical value of 1300 and 1400 appears to be appropriate. The following section will show that maximum range might be obtained with slightly more expansion, $P_5/P_O \sim 3$, where an I_f near 1500 would be appropriate.

Optimum Expansion for Lift

Lift coefficients are shown in Fig. 12, referenced to engine planform area, C_L, read from solid curves and left-hand ordinate, and to engine frontal area, $C_{L(A_F)}$ read from dashed curves and right-hand ordinate. These lift coefficients peak at higher P_5/P_O than do the thrust coefficients, because the ratio of lift to thrust increases as the initial flow angle leaving the cowl, θ_4, is decreased. In further explanation, the lift and thrust forces on the rear of the engine could be obtained in a different way by adding their respective components owing to the momentum of the burned gas leaving the cowl at station 4 and owing to the integrated pressure force over the expansion surface between station 4 and the trailing edge (refer to Fig. 7). Since the velocity vector V_4 has an upward component, the stream thrust which produces an equal and opposite force on the engine at this point has a downward component, hence $\vec{\mathcal{F}}_4$ contributes negatively to lift according to $\sin\theta_4$ and positively to thrust in proportion to $\cos\theta_4$. Moreover, as θ_4 is decreased, the lift component on the effusor surface owing to expansion of the burned gas will increase relative to the thrust component.

The lift coefficients must eventually pass through a maximum, with the present assumptions on cowl geometry (Appendix I), because both planform and frontal area increased area increase rapidly for $P_5/P_O > 10$, and in this region the cowl contribution to lift is an increasing negative quantity. On the other hand, for $P_5/P_O < 5$, the

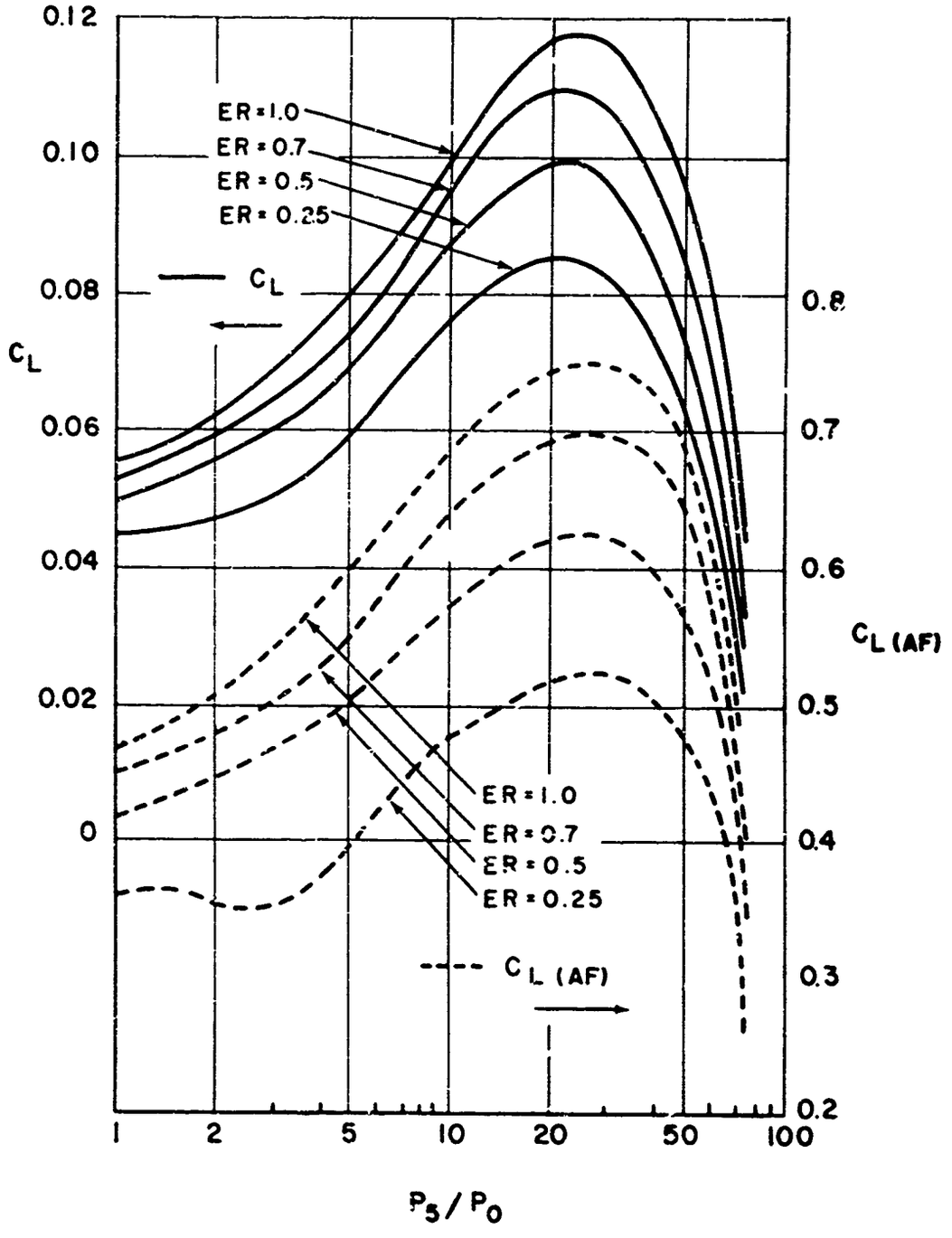

Fig. 12 LIFT COEFFICIENTS VERSUS P_5/P_0 FOR VARIOUS EQUIVALENCE RATIOS

C_L based on engine planform area; $C_{L(AF)}$ based on engine frontal area. Compare $C_{L(AF)}$ to $C_{T,NET}$ for relative lift and net thrust forces.

cowl presents an increasing positive contribution to the lift force, a case analogous to a conventional engine plus wing.

Relative lift forces, which include the cowl contribution, should be compared to net thrust forces through $C_{L(A_F)}$ and $C_{T,\ NET}$.

Effect of Equivalence Ratio on C_L

For an E.R. of ≤ 0.7, the effect of equivalence ratio on C_L is smaller than on $C_{T,\ NET}$, because as equivalence ratio is decreased, the velocity V_4 decreases (see Table II), and hence the adverse $\mathcal{F}_4$ effect on lift discussed in preceding paragraphs becomes smaller.

Lift/Drag Ratio for the Engine

If this engine could be stabilized more easily, particularly against the pitching moment resulting from the lift under the effusor surface (unless the c.g. is far to the rear), then it would provide a vehicle of very high L/D indeed. Figure 13 shows that a value of 15 is estimated for stoichiometric burning with $P_5/P_O = 8$. An L/D of 9 is estimated even for the lowest equivalence ratio, for which the corresponding net thrust coefficient would be only 0.1. However, these high L/D's could only apply for climb or acceleration; for constant velocity cruise the net thrust would have to be opposed by an added external drag.

Optimization for Range

The significance of the results of the foregoing calculations with regard to a long-range cruise vehicle can be better understood by considering the Breguet equation for maximum range at constant velocity.

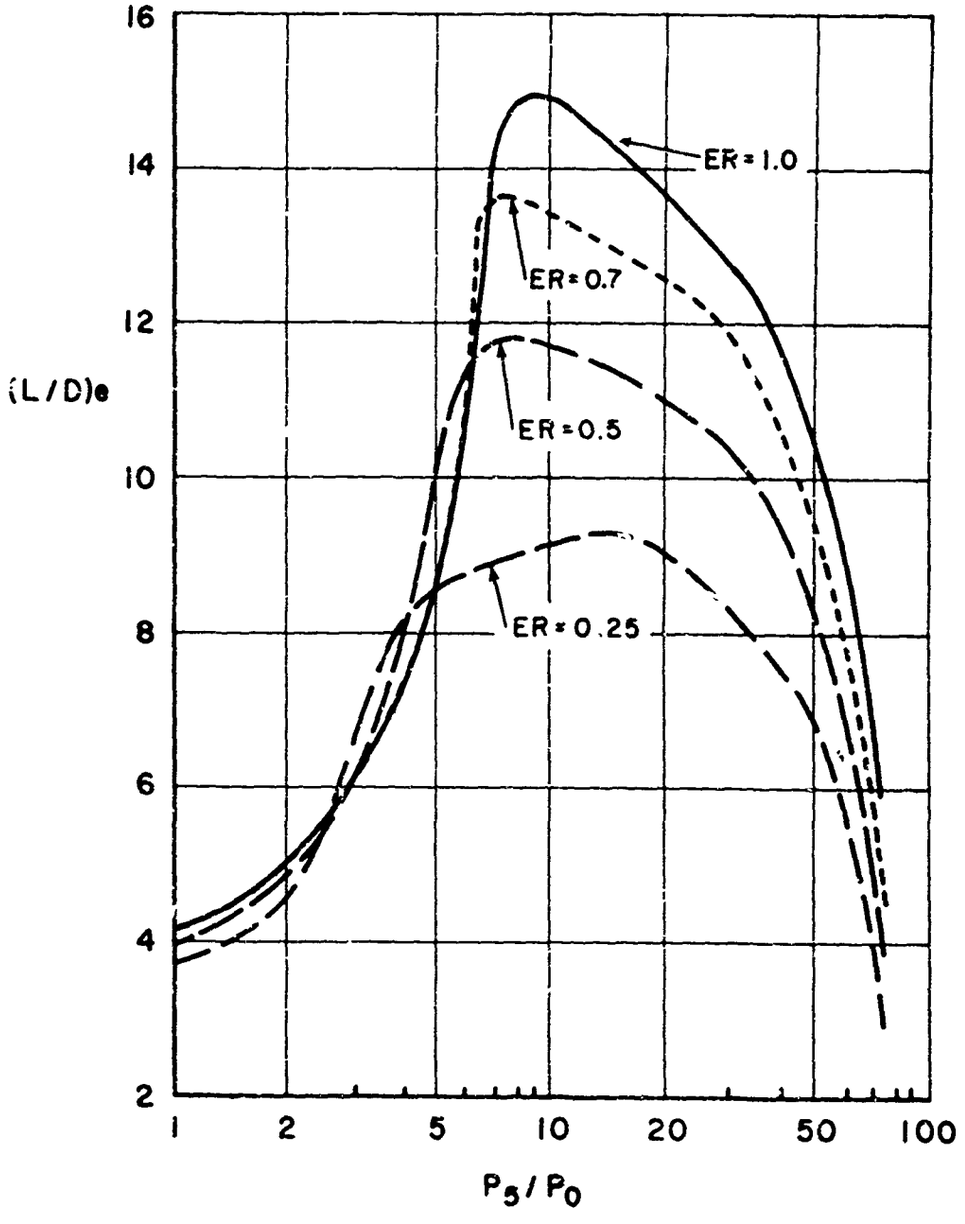

Fig. 13 ESTIMATED LIFT/DRAG RATIO FOR ENGINE VERSUS P_5/P_0 FOR VARIOUS EQUIVALENCE RATIOS

See Appendix I for cowl lift and engine drag assumptions.

$$R = V(I_f L/D) \ln (W_O/W_1)$$

In this equation thrust equals drag and lift equals weight. For maximum range, one wants to maximize the quantity $I_f L/D$. (If changes in $I_f L/D$ noticeably affect the logarithm of the initial to final weight ratio W_O/W_1, then one must maximize $(I_f L/D) \ln (W_O/W_1)$, but the latter refinement is beyond the scope of the present report. Centrifugal lift, which amounts to about 3.7 percent of vehicle weight at Mach 5, is also neglected.)

As a first approximation to a vehicle fulfilling the requirement of drag equal to thrust, it is assumed that the most economical way to increase drag is to add wings. An L/D of 6 for added wings is considered appropriate for Mach 5 cruise. The wing drag coefficient based on engine frontal area is assumed to be equal to the net thrust coefficient $C_{T,NET}$. The total lift coefficient based on engine frontal area is then taken to be the engine lift coefficient $C_{L(A_F)}$ plus six times $C_{T,NET}$. The resulting L/D for the missile is this total lift coefficient divided by the gross thrust coefficient (or total drag coefficient) C_T.

Figure 14 presents the total lift-drag ratios estimated in this way. An overall L/D of 6.0 to 6.5 in the region of interest for E.R. = 0.5 to 1.0 is indicated. (The E.R. = 0.25 curve runs off the plot to some maximum L/D near 12 at $P_5/P_O \simeq 30$; values for higher P_5/P_O are not of interest because I_f is negative.) These values may be compared with the L/D range of 4 to 5 often mentioned for a Mach 5 wing-body vehicle with a conventional ramjet to show that a 20 to 60 percent gain in L/D might be expected for a cruise vehicle with external burning.

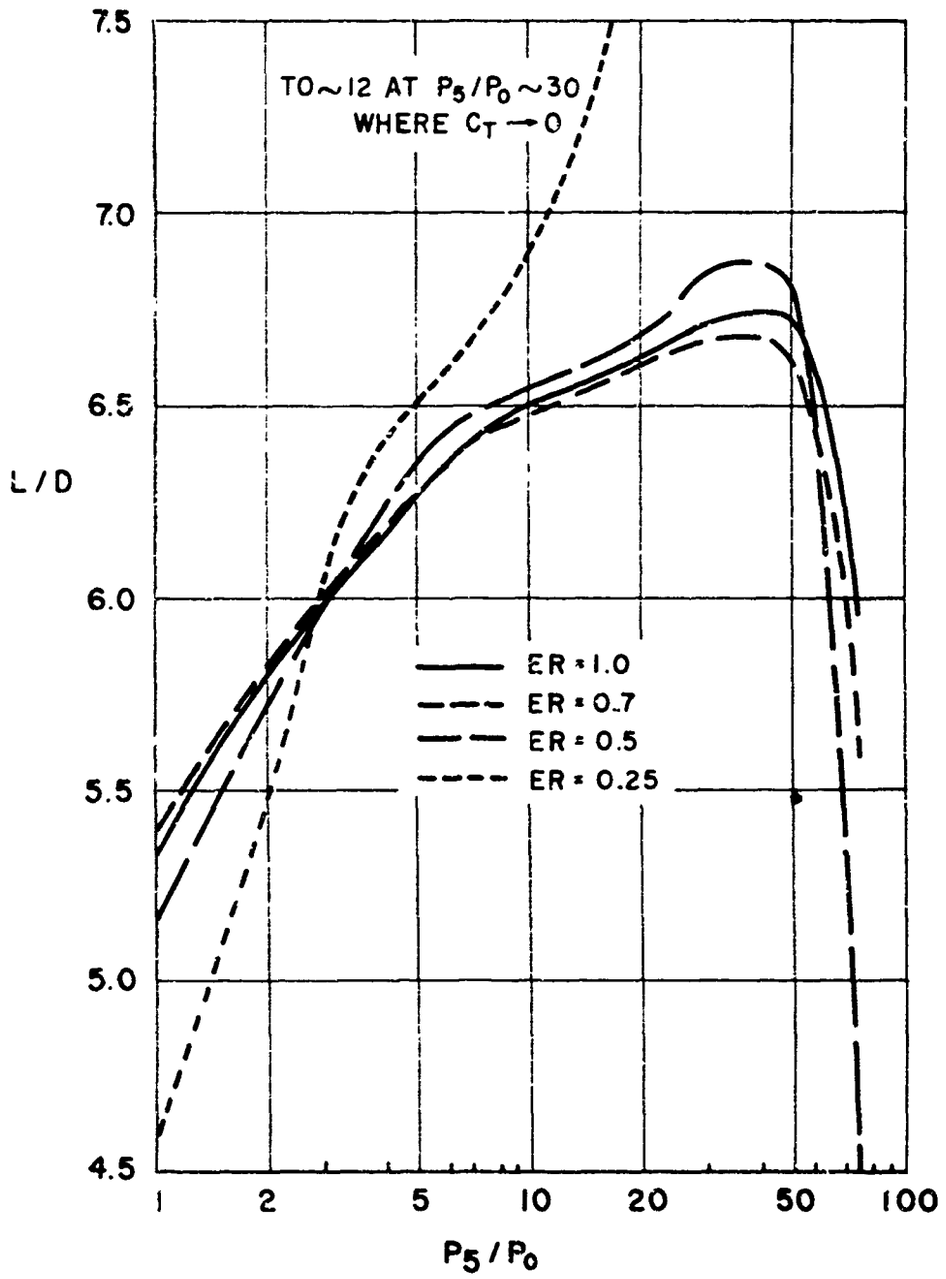

Fig. 14 OVER-ALL LIFT/DRAG RATIO FOR CRUISE VEHICLE WITH ZERO NET THRUST, BASED ON ADDITION OF WINGS OF L/D = 6

Figure 15 shows the range parameter, I_f L/D, for the engine-plus-wing vehicle using the above overall L/D. For each equivalence ratio, the maximum I_f L/D occurs at $P_5/P_O \sim 3$; this optimum pressure ratio becomes more sharply defined as the equivalence ratio is decreased. The highest I_f L/D calculated was 8850 for E.R. = 0.5 and $P_5/P_O = 3$, with values for E.R. = 0.7, 0.25, and 1.0 following in decreasing order. Apparently the optimum equivalence ratio would be near 0.6 and the corresponding I_f L/D would be 9000 ± 100.

On the basis of these calculations, an engine-plus-wing vehicle designed for cruise at Mach 5 at 100,000 feet with an equivalence ratio of 0.5 and $P_5/P_O = 3$ would have the following characteristics:

Minimum ratio of engine length to height, ℓ_t/h_F	= 7.8
Corresponding minimum engine body volume, vol/A_F	= 3.7 ft^3/ft^2
Percentage of lift contributed by engine	= 18 percent
W_O/A_F at start of cruise = $(C_{L,\ total})\ q_O A_{plan}/A_F$	= 1000 lb/ft^2
For 50 lb/ft^2 wing loading, wing area A_W/A_F	= 20 ft^2/ft^2
Lift/drag ratio in cruise	= 6.0
I_f L/D in cruise	= 8850 lb-sec/lb

Comparable values for the conventional ramjet of Table II with $C_v = 0.97$ and with added wings of L/D = 6 would be

I_f (with $C_v = 0.97$)	1600 lb-sec/lb
L/D in cruise	5.05
I_f L/D in cruise	8080 lb-sec/lb

Thus if W_O/W_1 were comparable for the two engines, the range for the conventional ramjet vehicle would be 8 percent smaller. A

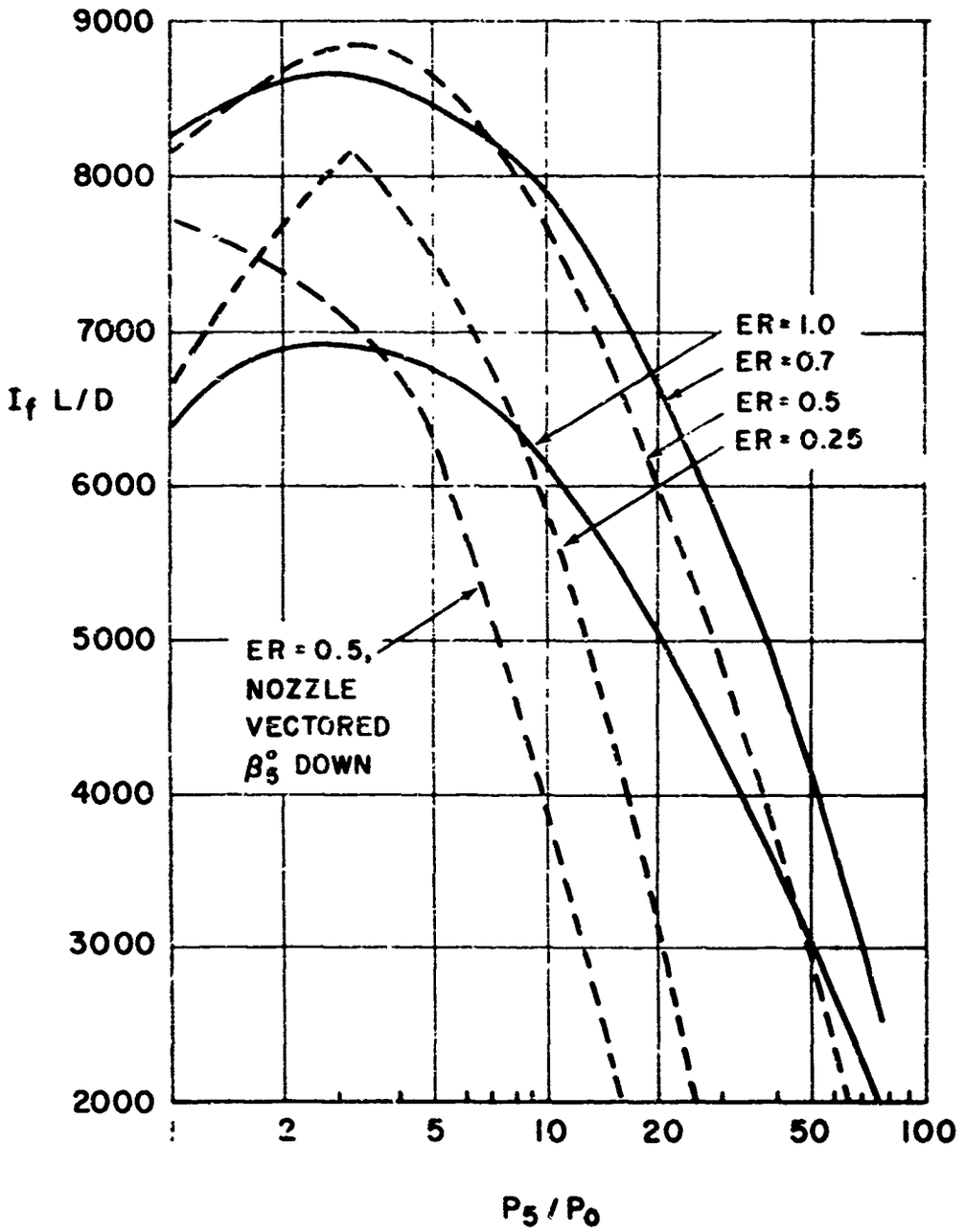

Fig. 15 OVER-ALL RANGE PARAMETER, I_f L/D, FROM FIGS. 11 AND 14

Included for comparison at E. R. = 0.5 is curve for effusor rotated downward through θ_5 degrees (last Mach line parallel to flight axis, θ

comparison of W_O/W_i is not readily made, because on the one hand the ERJ requires less added wing area per square foot of frontal area, less cooling water, and less nozzle surface area, but on the other hand two-dimensional engine construction would be heavier than axisymmetric construction.

One can see that if the engine body volume of the above ERJ vehicle were to represent the fuel storage and packaging space for the missile, the minimum-length engine could carry very little fuel per square foot of frontal area and would have a range of the order of 500 to 1200 nautical miles. The above numbers would therefore be appropriate only to small short-range missiles. However, if the body under the cowl is simply lengthened sufficiently to give an average fueled missile density of 80 lb/ft^3 at the beginning of cruise, then a new external drag coefficient applies, and the following characteristics are estimated.

Engine length of height ratio, ℓ_t/h_f	= 14.2 ft/ft
Engine body volume, vol/A_F	= 12.5 ft^3/ft^2
Lift/Drag ratio in cruise	= 5.73
I_f L/D	= 8420 lb-sec/lb
Cruise fuel, occupying 80 percent of body volume at 50 lb/ft^3, w_f/A_F	= 500 lb/ft^2
Cruise range	= 4700 n. miles

As noted previously, internal friction loss under the cowl is neglected. A rough estimate indicated $P_{t_3}/P_{t_2} \sim 0.958$, or $\Delta P_t/q \sim 0.39$, for the latter example. If one assumes that to a first approximation the exit thrust components are reduced in ratio to P_{t_3}, then I_f is reduced from 1470 to 1230 lb-sec/lb, and the range is reduced from 4700 n. miles to 3900 n. miles. This would still be an admirable cruise range for a

Mach 5 missile with, say, an engine 1.4 feet thick by 4 feet wide by 20 feet long, with 110 ft^2 of added wings and with a dry weight of 2800 pounds and a fuel capacity of 2800 pounds. Some 10 to 14 ft^3 of body volume would remain for payload and controls; this payload volume could be increased by carrying part of the fuel in the wings. Edge losses for the engine might be compensated by favorable wing-body interference effects in an integrated design (see also Section V). Use of a high energy fuel of 25 percent higher heat of combustion and 10 percent greater density would increase range 30 percent, raising the 3900 n. miles figure cited above to 5100 n. miles.

Effect of Vectoring Nozzle

For any given equivalence ratio and P_5/P_O, the lift coefficient can be increased at the expense of thrust coefficient by vectoring the after end of the engine downward. A few calculations were made to investigate the effect of vectoring on the overall I_f L/D. It was assumed that the isentropic external diffuser should be held at zero angle of attack for greatest efficiency, while the after end of the engine was rotated downward to put $\vec{V}_5$ at a positive angle of attack. However, for the cases calculated, the loss in I_f was always equal to or greater than the gain in overall L/D (with added wings) for that expansion ratio providing the highest product of I_f and L/D. In other words, the brief study made revealed no way to improve on the maximum overall I_f L/D which was calculated for the straight case with $\vec{V}_5$ parallel to the flight axis.

Figure 15 includes an I_f L/D curve calculated for an engine with the after end rotated downward through β_5 degrees, so that for each point on the curve the last Mach line is parallel to the axis and $\vec{V}_5$

makes an angle β_5 with the flight axis. The top surface of the engine is assumed to be "boattailed" at the angle β_5. (Refer to sketch at top of Fig. 16.) Only for P_5/P_O near unity does the vectored-effusor engine provide reasonable I_f L/D, and even at $P_5/P_O = 1$, the value produced is only 87 percent of the maximum I_f L/D for the "straight engine." Some improvement for the vectored engine could be obtained by streamlining the top surface at the expense of body packaging volume, but it is doubtful that it would produce higher I_f L/D than the straight engine.

Comparison with a Conventional Ramjet with Vectored Nozzle

On the basis of gross thrust versus lift force due to internal flow (that is, neglecting lift due to the cowl), the conventional ramjet and the external expansion ramjet, both with vectored nozzles, give nearly the same result for the same nozzle velocity coefficient and the same exit-to-ambient pressure ratio P_5/P_O. This is illustrated in Fig. 16 in which F_g/q_OA_O is plotted both against $L_{5_{net}}/q_OA_O$, where $L_{5_{net}}$ is "gage corrected" by subtracting the product of P_O and the horizontal projection of A_5 for each engine, and against L_5/q_OA_O where the "gage correction" has not been applied. The $L_{5_{net}}$ curve is essentially the same for both engines; the small advantage for the conventional engine owing to its lower total pressure loss for heat addition at lower subsonic Mach number (Table II) apparently is compensated with the ERJ by the fact that the gage pressure x area term in the lift force is greater. The difference between L_5 and $L_{5_{net}}$ is greater for the ERJ for the same reason, that is,

$$A_5 \cos(\theta_v - \beta_5)P_O = \text{gage correction for ERJ}$$

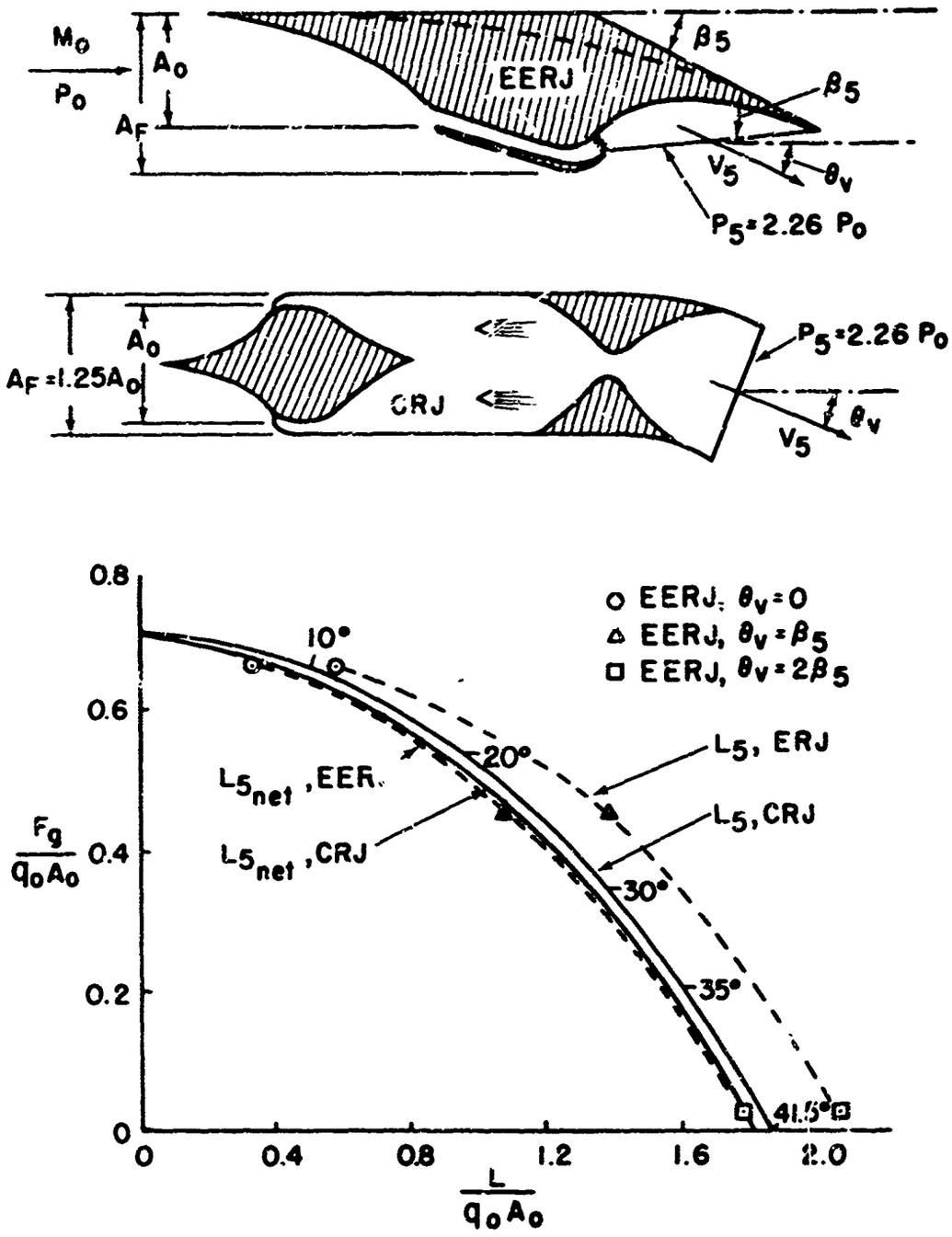

Fig. 16 VECTORED-NOZZLE RAMJET VERSUS VECTORED-EXPANSION-SURFACE EERJ: VARIATIONS OF GROSS THRUST AND NOZZLE LIFT COEFFICIENTS (BASED ON CAPTURE AREA A_0) AS NOZZLES ARE ROTATED DOWNWARD

is much greater than

$$(A_F = A_5)(\cos \theta_v)\, P_O = \text{gage correction for CRJ}$$

Obviously, if the ERJ is boattailed as sketched, the pressure on the boattail will be less than P_O, and it could be made still smaller by streamlining as suggested by the dashed line; moreover, the cowl will add to the lift. (Cowl lift was included in Figs. 12 through 15.) If the conventional ramjet is pod-mounted, then the pressure below its nozzle will also be greater than the pressure above its nozzle, so that the external surfaces will increase the overall lift and reduce the net thrust. It is likely that this effect would penalize a vehicle employing pod-mounted, three-dimensional conventional engines with vectored nozzles, whereas the cowl serves to increase the L/D of the two-dimensional ERJ at low to moderate P_5/P_O. If, on the other hand, the nozzle is inside a fuselage, these pressure effects probably would be eliminated. Thus the relative merits of the two vectored-nozzle engines with respect to lift and thrust will depend on how the engines are integrated with airframes. Further discussion on the integration of the EERJ with airframes is given in a later section.

Substitution of Simple Wedge Effusor

In connection with the foregoing calculations with ideal, nonreflecting expansion surfaces, it was pointed out that for $P_5/P_O > 10$, corresponding to flow turning angles less than one radian, A_e/A_O becomes small ($< 1/2$), so that the rear portion of the cowl becomes large even though the front was of the minimum dimensions. Such a cowl contributes negatively to lift while still introducing an appreciable drag.

In order to permit operation at smaller turning angles with a small, low-drag, low-cooling-requirement cowl, it might be desirable for some missions to compromise the thrust by substituting a simple wedge in place of the ideal effusor. A wedge-effusor engine would be simpler to construct, more adaptable to geometry variation to vary θ_4 of A_4, and would provide more packaging volume under the effusor and make it easier to control the c.g. to overcome pitch.

Figure 17 illustrates the flow model for wedge expansion. This sketch is oversimplified, because the Mach lines originating from the Prandtl-Meyer expansion around the cowl lip are actually curved before they reach the ramp, as a result of refraction by earlier Mach lines which have already been reflected from the surface. This may be seen in Fig. 18, which shows a portion of the graphical characteristics solution (obtained by the method described in Ref. 25) for each of three cases.

By comparing various cases in Figs. 18 and 19 one can see two effects which further enhance the refraction effect. Comparison of the ramp intercepts in Fig. 18 for the solid-line and dashed-line characteristics, representing incorrect use of the frozen sound speed a_f and correct use of the equilibrium sound speed a_e, respectively, shows that the latter characteristics have been refracted more for a given degree of turning at the cowl lip, and that the difference increases with distance. The second effect is due to greater refraction as equivalence ratio is increased, as may be seen by comparing the solid-line intercepts for E.R. = 1.0 to the dotted-line intercepts for E.R. = 0.5. The result on the normal force coefficient, $F_{5_n}/q_O A_O$, where F_{5_n} is the total normal force owing to expansion over a ramp of length ℓ is shown for

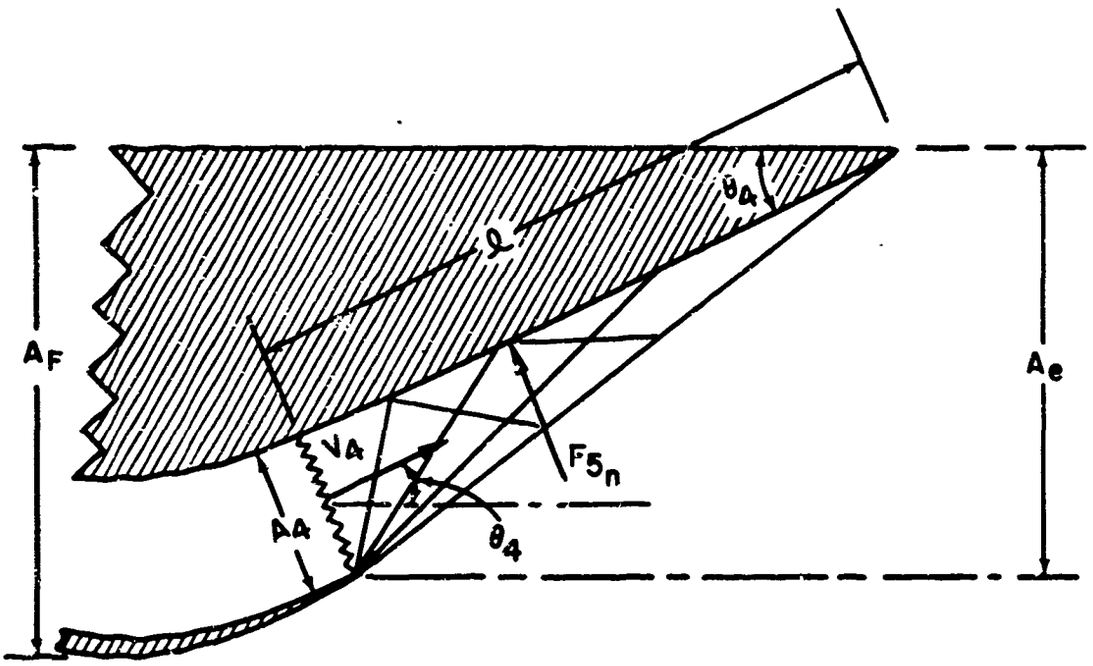

Fig. 17 MODEL FOR EXPANSION OVER SIMPLE WEDGE

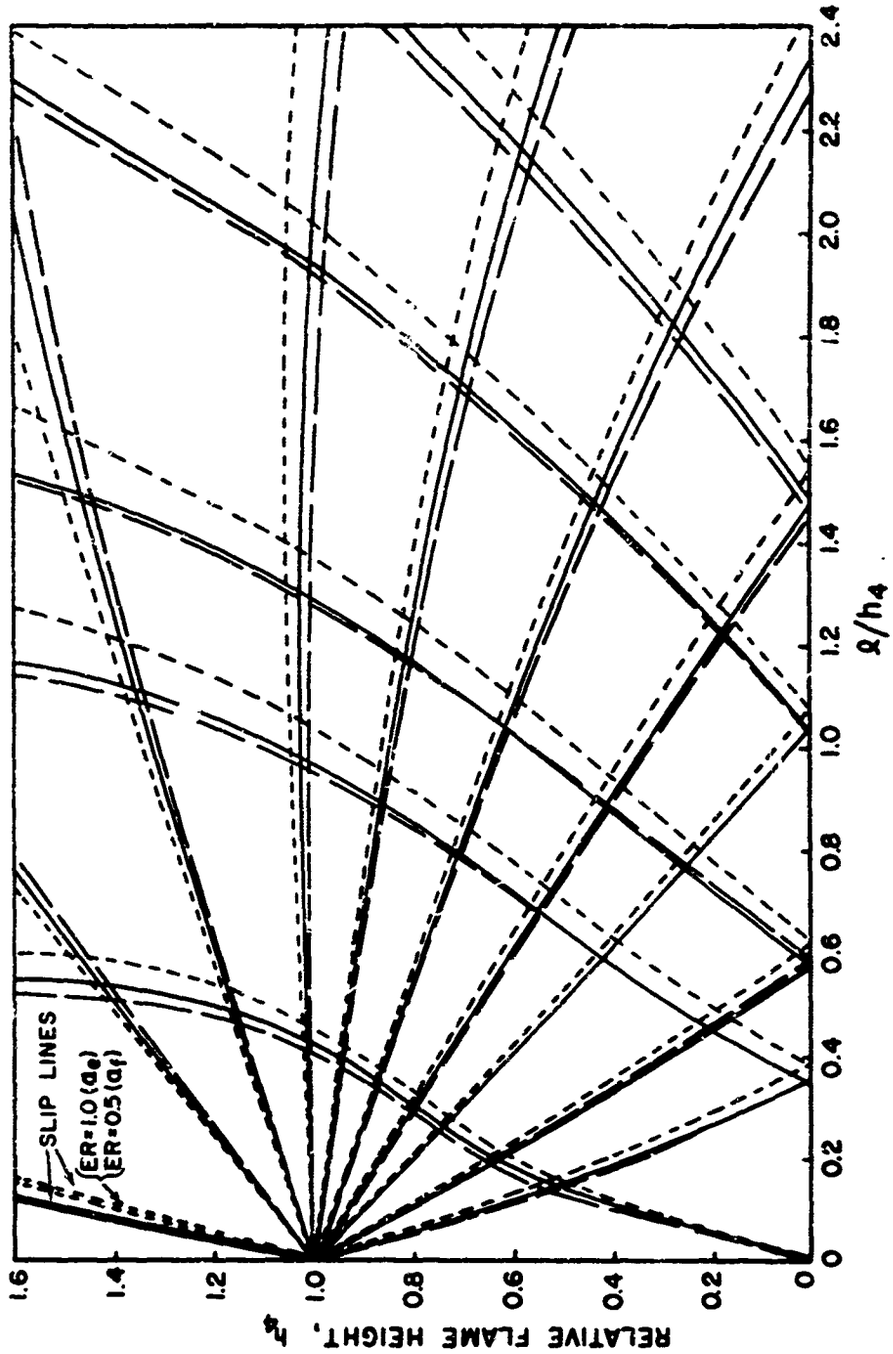

Fig. 18 REAL GAS CHARACTERISTICS FOR EXPANSION OVER SIMPLE WEDGE, ILLUSTRATING REFRACTION OF MACH LINES AND EFFECTS OF EQUIVALENCE RATIO AND OF a_f VERSUS a_e ON REFRACTION

—— ER = 1.0, a_f; --- ER = 0.5, a_f; — — ER = 1.0, a_e

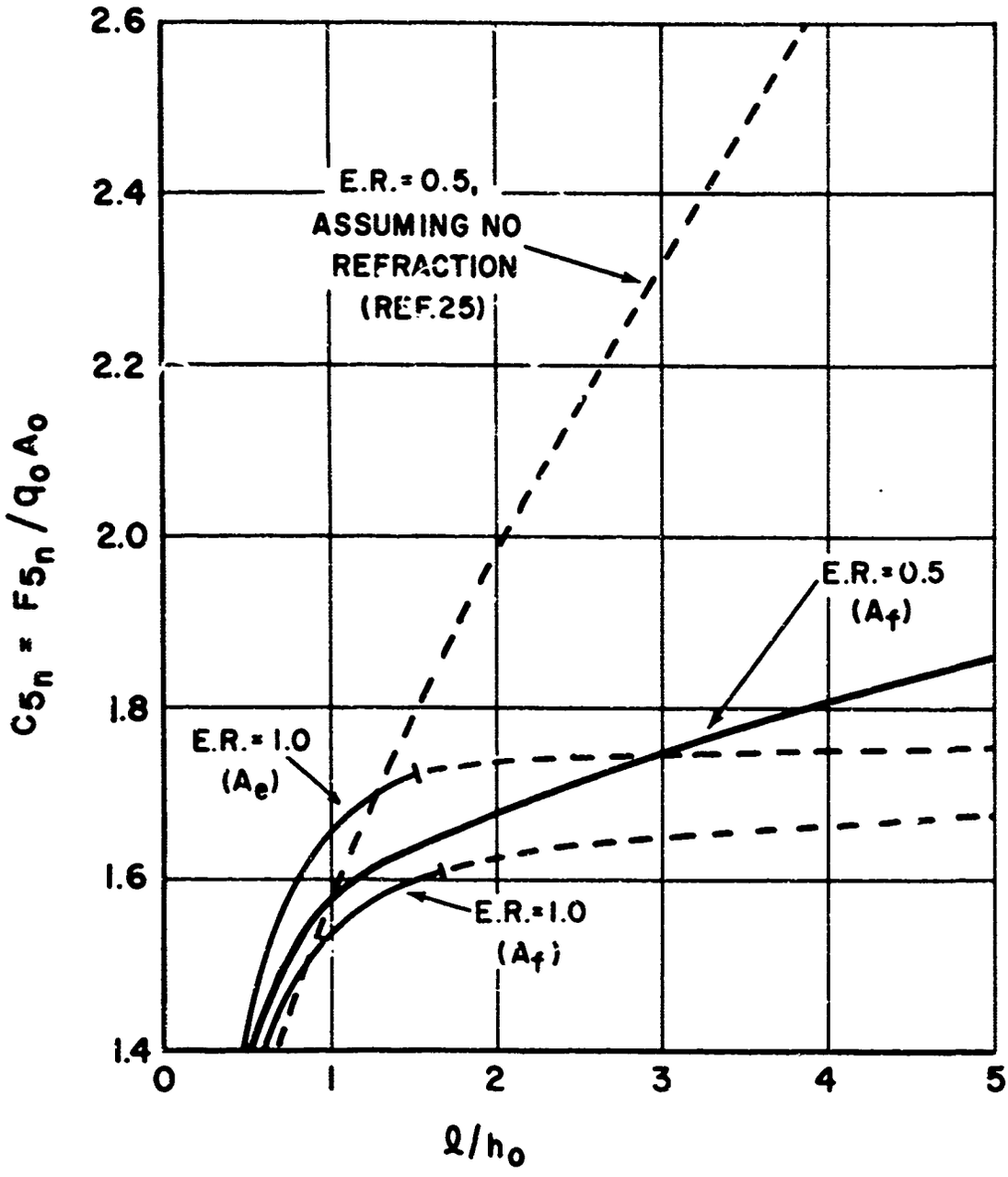

Fig. 19 COEFFICIENT OF NORMAL FORCE DUE TO EXPANSION VERSUS EXPANSION RAMP LENGTH FOR SIMPLE WEDGE-- EFFECTS OF REFRACTION

these three cases in Fig. 19 for the range of ramp lengths of interest. For E.R. = 1.0 the ambient pressure P_O is reached at $\ell = 1.52\ h_O$ (where h_O is capture height corresponding to A_O), so that greater lengths are of no interest for the equivalence ratio. Since the refraction effect is smaller at E.R. = 0.5, the greatest ℓ/h_O of interest is of the order of 5. A curve for E.R. = 0.5 based on the assumption that refraction can be neglected completely is also included for comparison to show why the wedge results obtained in this manner can be very misleading.

In order to present thrust and lift forces in terms of A_e/A_O, the following relationship is employed:

$$A_e/A_O = \ell \sin\theta_4 + (A_4/A_O)\cos\theta_4 \qquad (20)$$

A stream thrust analysis shows that the gross thrust will now be given by

$$F_g = F_{5_n} \sin\theta_4 + \mathcal{F}_4 \cos\theta_4 - \mathcal{F}_O - P_O(A_e - A_O) \qquad (21)$$

where

$$F_{5_n} = C_{5_n} q_O A_O$$

and

$$\mathcal{F}_4 = P_4 A_4 (1 + a_{e_4}{}^2/R_4 T_4) \qquad (22)$$

and the lift force on the configuration will be

$$L = L_{5_{net}} + L_4 + L_{c_{net}} \qquad (23)$$

where

$$L_{5_{net}} = (F_{5_n} - P_O \ell)\cos\theta_4 \qquad (24)$$

and

$$L_4 = -\mathcal{I}_4 \sin \vartheta_4 \qquad (25)$$

and $L_{c_{net}}$ is again calculated as in Appendix I.

The results are summarized in Table III. The highest overall $I_f L/D$ calculated was 5190 for $\theta_4 = 0.524$ rad (30°) in the series in which A_F was held constant at the minimum value (determined by the 10° diffuser lip) of 1.008 A_O. For this turning angle of 30°, P_5/P_O is near unity (approximately 0.9), so that no further expansion would be realistic. The value of 5190 for $I_f L/D$ is only 75 percent of the maximum value of 6900 calculated for the isentropic ramp model at this equivalence ratio.

It is therefore concluded that a simple wedge effusor would not be chosen for a maximum range vehicle, although the other advantages mentioned previously might well lead to its choice for short range missiles or for higher velocity missiles in which the structural and/or cooling problems associated with a long cowl might outweigh the loss in propulsion performance.

Table III

Results for Simple Wedge Effusor

(Kerosene, E.R. = 1.0; characteristic solution for surface pressure; conditions through station 4 same as in Table II; $C_V = 0.97$.)

θ_4 (rad)	$\frac{A_f}{A_O}$	$\frac{A_e}{A_O}$	$\frac{P_5}{P_O}$	C_T	$\frac{I_f}{\frac{lb}{lb/sec}}$	C_L	$\frac{L}{D}_e$	With added wings for $C_{T_{NET}} = O$	
								$\frac{L}{D}$	$I_f \frac{L}{D}$
0.524	1.008	0.917	0.9	0.751	848	0.287	9.0	6.12	5190
0.550	1.008	0.908	1.3	0.752	850	0.214	6.7	6.02	5120
0.600	1.008	0.890	1.7	0.763	863	0.074	2.3	5.83	5030
0.700	1.008	0.849	2.7	0.749	846	-0.214	-6.3	5.45	4610
0.800	1.008	0.802	4.6	0.697	788	-0.504	-14.4	4.98	3930
0.600	1.119	1.000	1.0	0.765	865	0.125	2.8	5.81	5020
0.700	1.159	1.000	1.6	0.758	857	-0.096	-1.8	5.48	4700
0.800	1.205	1.000	2.3	0.721	815	-0.300	-5.4	5.13	4180

IV. RANGE-WEIGHT COMPARISON OF ERJ WITH OTHER MISSILES 1500-POUND USEFUL PAYLOADS

Figure 20 compares predicted weight-range performances for four ballistic rocket alternates, one glide rocket, and three ramjet alternates, the last of which would incorporate external burning. The assumptions used to calculate these curves are discussed below.

General Assumptions

1. In assigning useful payload weights for the rockets, it was assumed that half of the nose cone weight is payload (warhead) and half metal parts plus protection (see also item 7). For the ramjet, because of scaling requirements, it was necessary to restrict the analysis to one useful payload (or warhead) weight of 1500 pounds. The weight of the guidance for the ramjet was assumed to be independent of range. Thus the ramjet curves would vary if useful payload weight were changed. The ramjet weight advantage would increase for bigger payloads or decrease for smaller payloads.
2. All rockets follow the optimum trajectory for maximum range, and all ramjets follow the Breguet trajectory for maximum range after rocket boost to Mach 5 at 100,000 feet.
3. Ratio of initial weight to burnout weight for each rocket stage in a given missile is constant, but I_{sp} for the second

APPLIED PHYSICS LABORATORY
THE JOHNS HOPKINS UNIVERSITY
SILVER SPRING MARYLAND

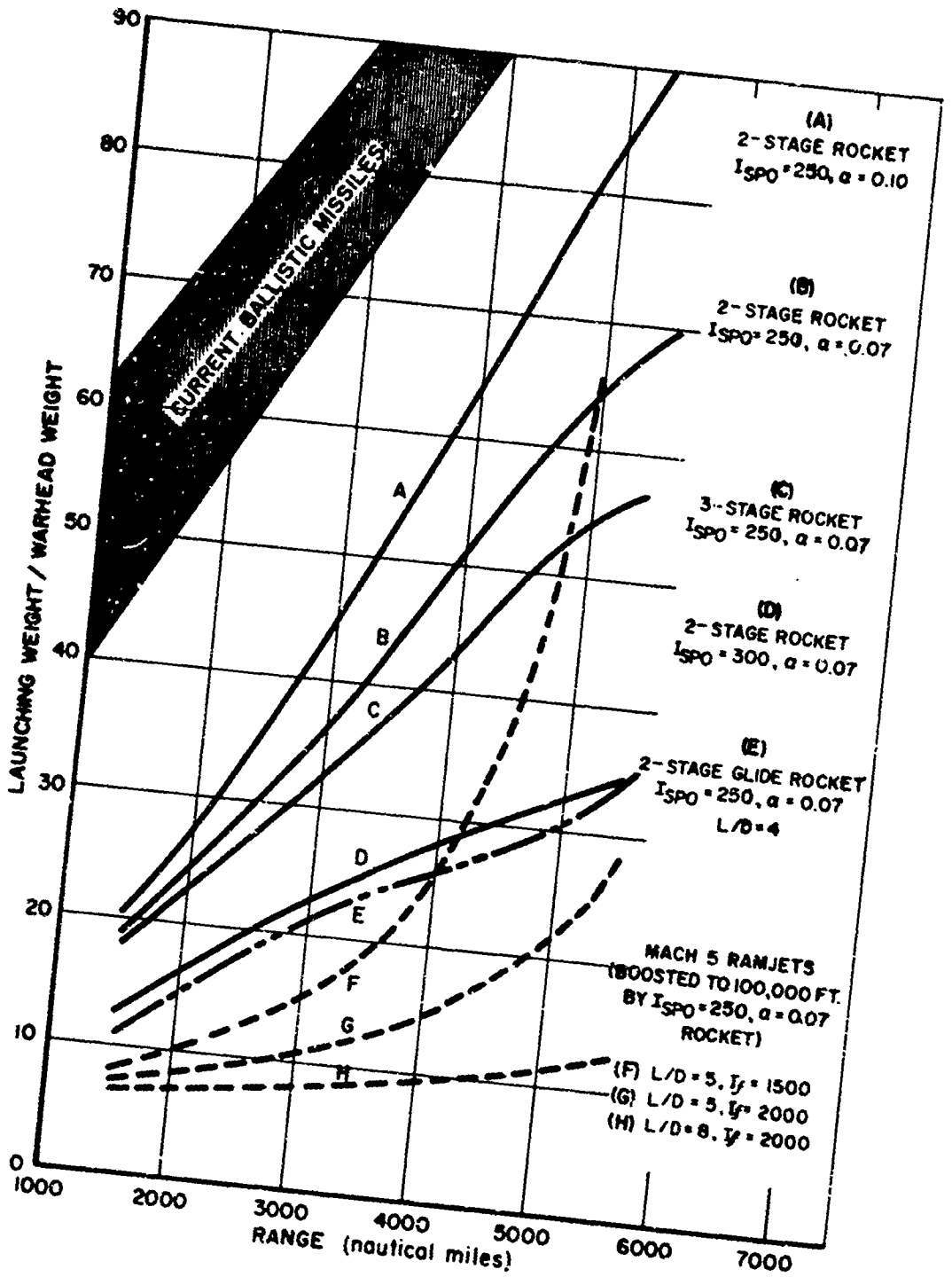

Fig. 20 PREDICTED WEIGHT-RANGE PERFORMANCE OF LONG-RANGE MISSILES CARRYING 1500-POUND WARHEADS

(and third) stage is assumed to be 20 percent greater than the effective I_{sp} of the first stage (to allow for greater thrust at higher altitude), so that the velocity increment for the second (and third) stage is 20 percent greater than the velocity increment for the first stage. A 3 percent drag allowance is made for the first stage so that $I_{sp_1} = 0.97\, I_{sp_o}$, and $I_{sp_2} = I_{sp_3} = 1.2 \times 0.97\, I_{sp_o}$. To achieve these impulses, it is assumed that the first stage nozzle has an expansion ratio near four and the second (and third) stage has an expansion ratio of 20 to 30.

4. Each missile has an initial acceleration of 4g's.

5. The basic rocket stage of the near future is assumed to be a solid propellant rocket of $I_{sp_o} = 250$ lb-sec/lb and structure/fuel weight ratio $\alpha = 0.07$. These values are used for curves A, B, C, and E and for the boosters for ramjet curves F, G, and H.

6. The probable practical limit for liquid propellant stages of the near future is assumed to be $I_{sp_o} = 300$ lb-sec/lb (estimated maximum delivered I_{sp} for fluorine-hydrazine) and $\alpha = 0.07$. This α value is believed to be the realistic goal for rockets of the size indicated by Curve D (that is, rockets much smaller than Atlas) when realistic allowances are made for the minimum control weight, fuel residues, and pressurization residuals which must be assigned to each stage. Indeed, some writers now feel that α for solid rockets may in the future be less than α for liquid rockets of comparable total impulse. A factor contributing to this

belief is that higher solid propellant density assures higher thrust per unit volume for the solid rocket.

7. For the glide rockets of Curve E, and L/D of 4 was assumed which may be "about right" if a second stage such as suggested by Eggers, et al., (see Fig. 12, Ref. 26), proves to be practical. This suggested design is simply a conical-nosed body with adjustable petal-type control surfaces at the after end. The vehicle would have relatively low drag during climb and low aerodynamic heating during glide. However, the addition of even these simplest variable control surfaces would, because of the severity of aerodynamic heating on the control surfaces, add appreciably to the glide vehicle weight. The glide vehicle weight is, of course, the payload of the rocket necessary to accelerate the overall missile. A 20 percent increase in the metal parts or coolant load of the glider would increase the launching weight 7 percent. This fact was considered in computing Curve E. The burn-out velocity versus range relationship used to obtain the curve was taken from Eggers, et al.

8. The ramjet curves are based on a relative weight breakdown for an advanced ramjet missile, with structures assignable to the payload scaled up to a 1500 pound payload weight and with cooling water, dive fuel, and related structures scaled to total ramjet stage weight. One-half pound of airframe weight was added for each pound of cruise fuel.

9. The fuel specific impulses chosen for the ramjets are believed to be realistic for kerosene ($I_f \sim 1500$ lb-sec/lb at

Mach 5) and HEF-3 ($I_f \sim 2000$ lb-sec/lb at Mach 5). These values correspond to an overall thermal efficiency of 0.5. On the assumption of a nearly constant thermal efficiency, the product of VI_f remains constant for higher Mach numbers, so that if L/D be constant, these same curves are approximately representative for higher ramjet cruise speeds, for example, to M = 10.

10. The lift-drag ratios assumed for the ramjets are: 5 for a conventional missile at Mach 5, and 8 for an advanced missile which would obtain part of its lift from external burning. Since an I_f L/D of 9000 seconds was estimated for external burning of kerosene at an E.R. of 0.6 in the previous section, the present use of I_f L/D = 2000 x 8 = 16,000 seconds for a well-designed, high-energy fueled engine is not unreasonable, particularly when one remembers that no credit for engine weight reduction is being given to curve H.

Conclusion

In general, the conclusion available from this figure is that for a broad and important span of flight distances the ramjet has an appreciable gross-takeoff-weight advantage over the rocket or glide rocket. That is, for equal payloads, the gross takeoff weight of the ramjet will be appreciably less than that of either the glide or ballistic rockets. Possible comparisons available from Fig. 20 are shown in Table IV.

Table IV

Comparison of Various Rockets and Ramjets,
Long-Range Missiles Carrying 1500-Pound Warheads

Rocket	Ramjet	Compare Curves	Remarks
2-stage, solid $I_{sp_o} = 250$, $\alpha = 0.07$	JP-5($I_f = 1500$) L/D = 5	B - F	Ramjet has 1:2 weight advantage to ranges of 4000 n. m., equivalent at 5000 n. m.
2-stage, solid	HEF($I_f = 2000$) L/D = 5	B - G	Ramjet has 1:3 weight advantage, 1500 to 5500 n. m.
2-stage, solid	HEF($I_f = 2000$) L/D = 8	B - H	Ramjet using external burning has 1:6 weight advantage.
2-stage, liquid $I_{sp_o} = 300$, $\alpha = 0.07$	HEF($I_f = 2000$) L/D = 8	D - H	The advanced ramjet with external burning has a 1:3 weight advantage over even the advanced liquid-fueled rocket. Note that for proper comparison, the ramjet would be boosted by a liquid rocket, which would lower (improve) any ramjet curve 15 percent.
2-stage, glide, solid	JP-5, L/D = 5	E - F	Ramjet obtainable with current technology still superior at ranges less than 4000 n. m. Note that gliding descent would add an additional 100 n. m. to ramjet range.

V. DESIGN PHILOSOPHY FOR HYPERSONIC EERJ TRANSPORT AIRCRAFT

The primary advantage which an external expansion ramjet would have over a conventional ramjet in hypersonic flight is the heat relief gained through radiation from the surfaces adjacent to the burned gases. In addition, a signal advantage accrues from conversion of the bursting forces produced in a ducted nozzle into a useful component of lift when the burned-gas expansion takes place solely on the under side of the vehicle. Consequently, the EERJ must be an integral part of the main body or wing, and no pod-type, thrust-generating devices should be permitted to complicate and vitiate the basically clean design. A type of flying wing is thus indicated.

Apart from the question of integrating the propulsion and aerodynamic features of the hypersonic ensemble, the greatest obstacle to practical accomplishment of such a high-speed vehicle is the extreme range of flight conditions to be met. It is assumed that the transport must take-off and land on its own power, and besides, it must pass through the transonic and lower supersonic Mach number range before the variable geometry EERJ can become operative (at about Mach 3) to provide acceleration to approximately Mach 7-10, where the cruise flight will be maintained.

Since there is neither adequate design information for variable inlets capable of operating at hypersonic speeds nor any backlog of experience on combustion processes under hypersonic flight conditions, no unique optimum aircraft design can be visualized. Three versions

of hypersonic jet transports ("idea airplanes") which incorporate turbojet engines for take-off and landing and ERJ engines for high-speed flight have been considered qualitatively. These are illustrated in Figs. 21 through 24.

The first version incorporates a delta wing, which has the desirable property of exhibiting very little center of pressure movement with variation in Mach number from low subsonic to hypersonic speeds. Inasmuch as the center of gravity will not normally change its position markedly during the course of the flight, it is desirable to select such a design giving constant c.p. location, in order to lessen the stability and control difficulties which would otherwise be encountered. However, in order to achieve low-speed landing this delta-wing version depends on large wing area, lightly loaded. To overcome the resulting large drag, the turbojet thrust required for take-off and acceleration will be large, and required turbojet engines become dead weight and volume wasters for the high-speed flight portion of the plane's trajectory. The state of development of the auxiliary turbojets thus has a direct bearing on the ultimate design of a truly versatile ERJ hypersonic design. Figures 21 and 22 show take-off and cruise configurations.

Although the delta wing, in the absence of variant combustion pressure fields, would appear to be an admirable choice for a versatile multi-speed-range aircraft, it may be found that the stability deteriorates under burning conditions. Consequently, the other line of approach to the attainment of trustworthy dynamic response at all speeds is to provide a configuration which can circumvent, by adequate control, the expected severe c.p. changes. The second version has a tandem monoplane (libellula) configuration which has the advantage of equally disposed lifts (both operating in the effective upward direction) which

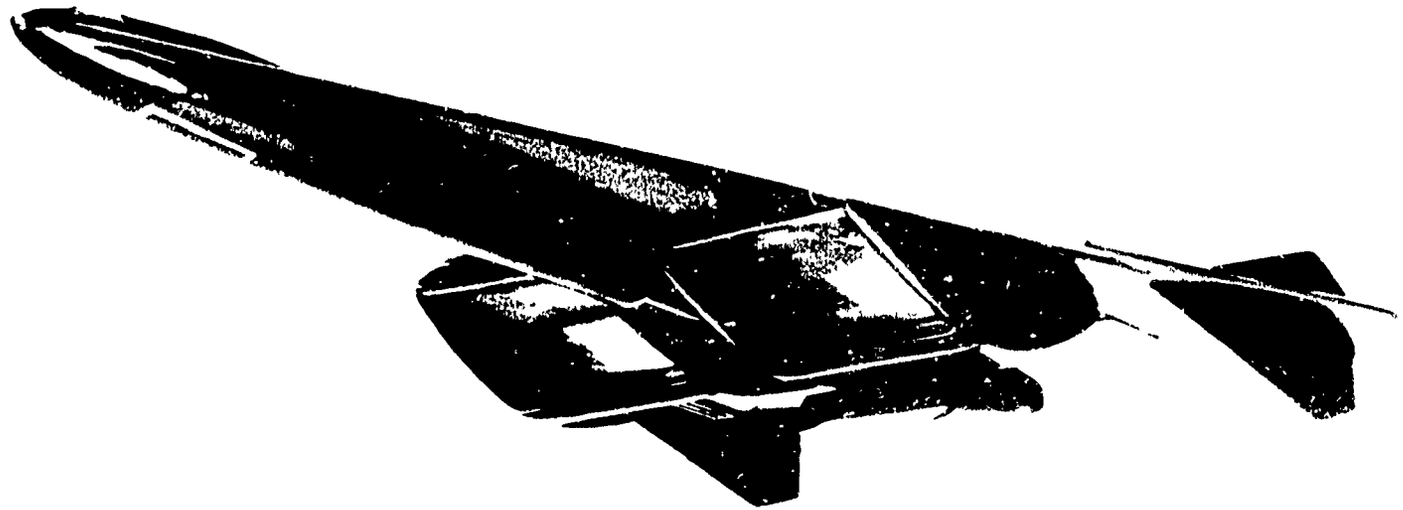

Fig. 21 DELTA PLANFORM VEHICLE IN TAKE-OFF CONFIGURATION

Fig. 22 DELTA PLANFORM VEHICLE IN CRUISE CONFIGURATION

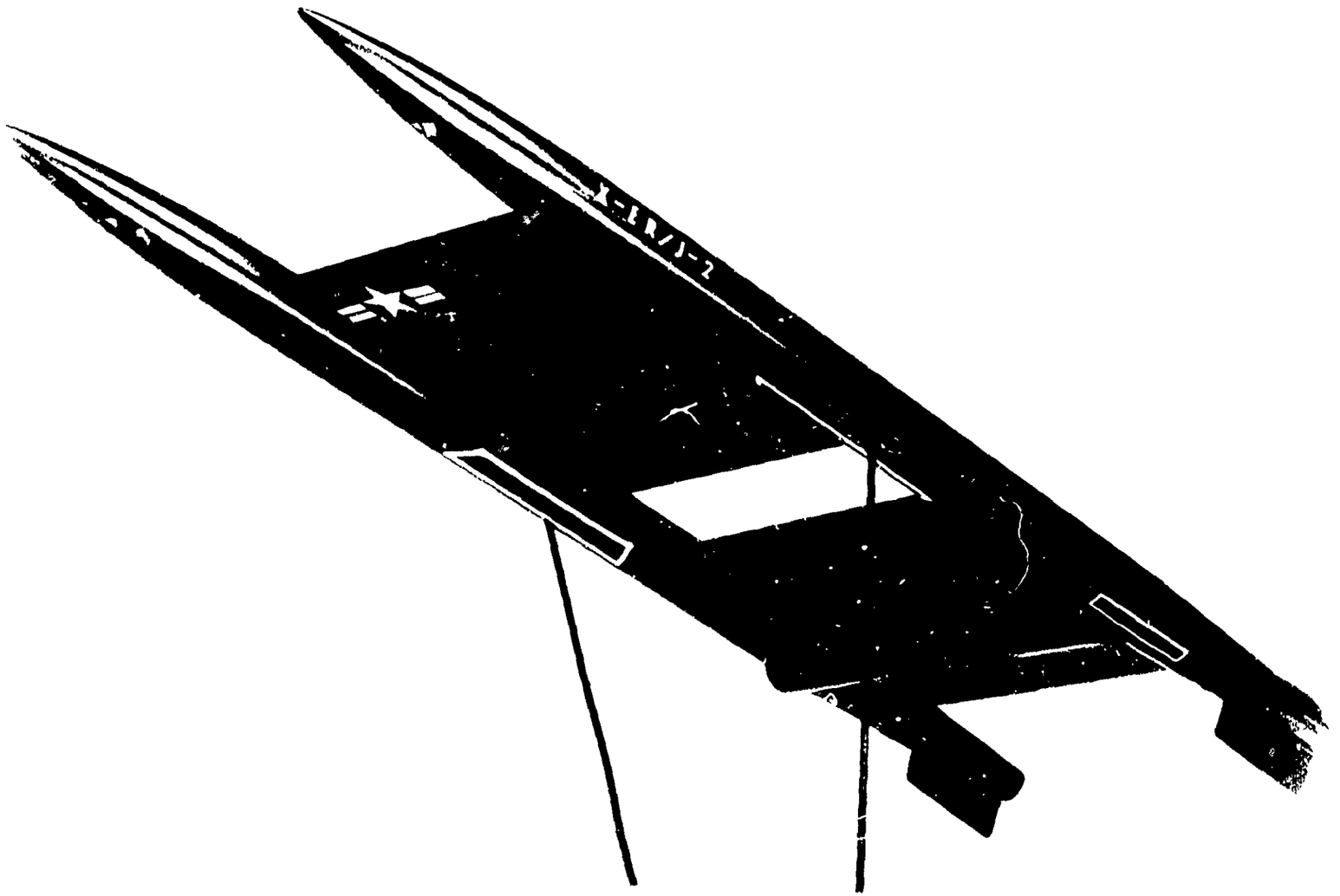

Fig. 23 TANDEM MONOPLANE (OR HIGHLY STAGGERED BIPLANE) USING TWO ERJ's BETWEEN TWIN FUSELAGES

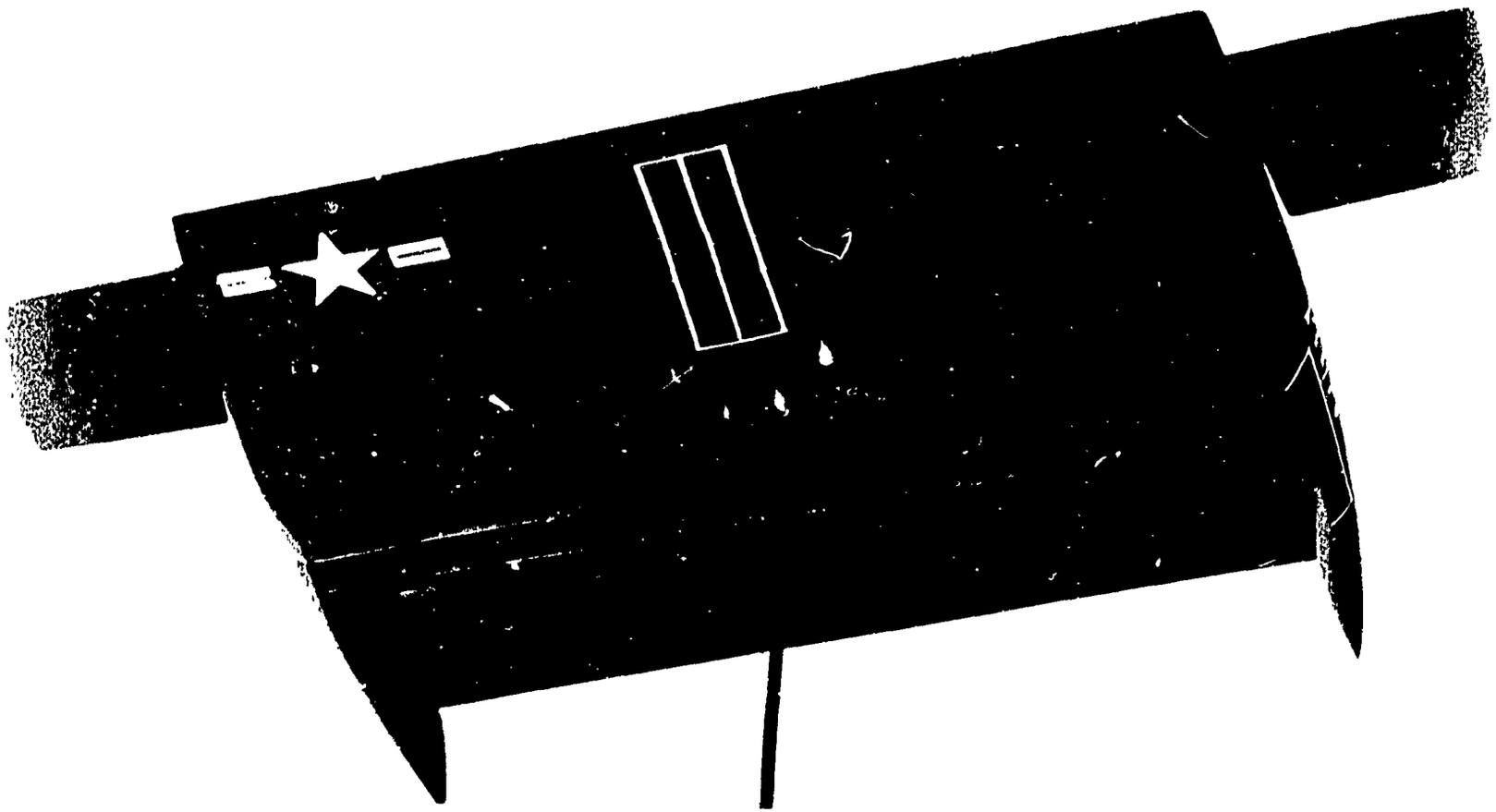

Fig. 24 COMPACT "FLYING WING" VEHICLE IN TAKE-OFF CONFIGURATION WITH PECTORAL WINGS EXTENDED

may be adjusted by the aid of spoilers or flaps to provide a very large margin of total airplane c.p. travel, more than obtained in any other design having a feasible tail length. The slot between the fore and after wings also acts to provide ultra-high circulation for slow speed landing. Severe transition problems occurring while converting from low to high speed flight configuration may be anticipated. Figure 23 is an upward view.

The third model, which represents attempts to eliminate fuselage fairings and provide a more compact design (passengers seated within the wing itself) would be a most efficient hypersonic-flight vehicle, but the c.p. variations over the speed range may be too excessive to be dealt with by conventional controls. Extra wing area is provided by laterally sliding pectoral flapped planes, and this fore-area control versus the large after flap, with circulation-control blowing-slots at its entrant edge, may be sufficient to overcome the anticipated large c.p. changes. Figure 24 is a 3/4 front view, which shows the pectoral flapped planes extended for landing.

In regard to the requirement for thrust generation through a wide range of speeds, it is believed that a hypersonic air-breathing vehicle will necessarily incorporate some variable geometry at the expense of structural complexity. The delta-wing model illustrates the concept of varying the shapes and positions of the main compression and expansion surfaces of the ERJ while holding the subsonic diffusion cowl fixed. The two straight-wing models rely on the supposition that the air flow area between the compression-ramp-and-effusor surface and the outrigger vane provides an adequate control variable, which is varied simply by extending the vane supports. Although this expedient obviates some structural, insulation and fuel-supply problems, it

implies toleration of nonoptimum jet operation· whether off-design performance of the EERJ will deteriorate catastrophically cannot be predicted at present. High drag in the base section of the EERJ is also to be expected at low speed.

In any event, there are many problems associated with the details of the flow in the EERJ and with such full-gamut speed-range aerodynamic ensembles, so that no hard and fast decisions as to the main features of such a hypersonic vehicle can be made at this time. The proposed models merely suggest that there are apt to be a variety of ways in which the ERJ principle can be wedded to hypersonic aerodynamic shapes to provide the performance capabilities foreseen from theoretical analyses.

THE JOHNS HOPKINS UNIVERSITY
APPLIED PHYSICS LABORATORY
SILVER SPRING MARYLAND

APPENDIX I

Method of Estimating Frontal Area A_F, Cowl Wave Drag Coefficient C_{D_c}, Friction Coefficient C_F, and Lift Coefficient C_L

It is assumed that the curved parts of the fore and after cowl surfaces approximate cylindrical surfaces having radii equal to four times the local duct heights, which correspond to areas A_2 and A_4, respectively. The remaining part of the cowl is assumed to be a plane surface tangentially extending either the front or rear cylindrical surface, depending upon the geometry dictated by θ_4 and A_e. In all cases it is assumed that the leading edge of the cowl makes an angle of 10° with the flight axis. (See Fig. 25.)

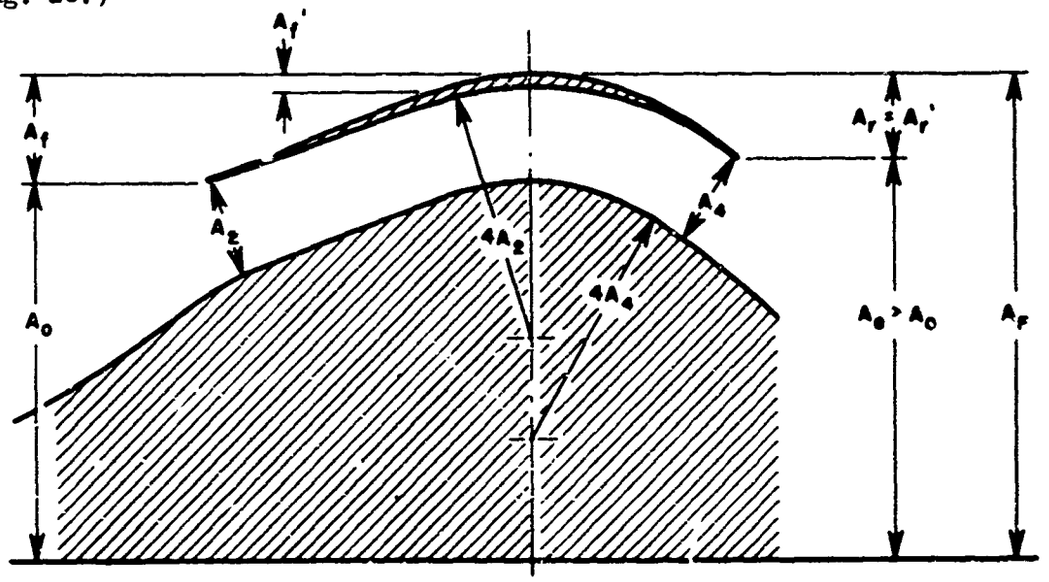

Fig. 25 ASSUMPTIONS ON COWL GEOMETRY

If A_f' and A_r' are defined as the minimum projected areas required to turn the flow from -10° to 0° and from 0° to θ_4, respectively, then

$$A_f' = 4A_2 (1 - \cos (10°))$$

$$A_r' = 4A_4 (1 - \cos \theta_4)$$

From the geometry it may be seen that when

$$A_e < (1 + A_f' - A_r'), \quad A_f = A_f' \text{ and } A_r = 1 + A_f' - A_e$$

but when

$$A_e > (1 + A_f' - A_r'), \quad A_f = (A_e + A_r' - 1) \text{ and } A_r = A_r'$$

The maximum cross-sectional area for the body plus cowl is the frontal area:

$$A_F = 1 + A_f = A_e + A_r$$

The pressure P_{c1} on the front surface or lip of the cowl is that behind the oblique shock for $M_O = 5$ and the 10° leading edge angle; $P_{c1}/P_O = 3.013$.

It is assumed that the flow separates on the rear surface and that the pressure there is $0.5\ P_O$. With these assumptions, the cowl wave force F_c is estimated by:

$$F_c = (P_{c1} - P_O)\ A_f - (0.5\ P_O - P_O) A_r$$

$$= (2.013\ A_f + 0.5\ A_r)\ P_O$$

and the cowl wave drag coefficient is given by

$$C_{D_c} = F_c / q_O A_F = (2.013 A_f + 0.5 A_r) P_O / q_O A_F$$

The external friction drag was crudely estimated using the relationship for laminar boundary layer flow

$$C_f \sqrt{R_\ell} \simeq 1.2 \text{ at Mach } 5$$

from Hoerner, Ref. 27 (p. 17-3). The Reynolds number per foot, R_ℓ / ℓ, was calculated to be 1.5×10^4 for the free stream conditions of 395°R and 0.01 atmosphere at Mach 5; it was assumed that to a first approximation the above relationship could be applied directly to both the top surface ($R_\ell = 1.5 \times 10^4 \ell_{total}$) and the cowl ($R_\ell = 1.5 \times 10^4 \ell_{cowl}$), and that the sum of the two C_f's so calculated would approximate C_f for the engine; each of the C_f's was related to engine frontal area by multiplying by the appropriate length, ℓ_{total} or ℓ_{cowl}, divided by A_F.

The cowl lift force is estimated from

$$L_{C_{net}} = (P_{c1} - P_O)[4A_2 \sin(10°) + (A_f - A_f') \cot(10°)]$$

$$+ (0.5 P_O - P_O)[4A_4 \sin\theta_4 + (A_r - A_r') \cot\theta_4]$$

$$C_L = L_{c_{net}} / q_O A_F$$

APPENDIX II

Validity of Prandtl-Meyer Expansion Calculations of Section III

In Section III it is assumed that the burned gas may be turned through a Prandtl-Meyer expansion to the point $\theta_5 = 0$ (flow parallel to top surface of missile) for final pressures as low as ambient, $P_5/P_O = 1$. At the same time, for the purpose of engine drag estimates, it is assumed that there is a separation region on the rear end of the cowl in which the pressure is approximately one-half of the ambient pressure P_O. In order to be satisfied that the Prandtl-Meyer expansion calculations are valid, the following models have been considered for the interaction between the burned gas and the external air stream.

In all probability there is a separation region or recirculation zone initiated from some point C on the cowl, as shown in Fig. 26(a). The first case to be considered is that in which the pressure in the recirculation zone decreases from P_O at point C to some lower but constant pressure along the line AB. The burned gas must be turned until pressure equals the pressure along AB, and the external air flow must also be turned and accelerated so that its pressure matches the decreasing pressure along CB. The external air flow and the burned gas flow meet at B; both flows must be turned to equalize pressures and directions. The slip line between the flows is labeled BD. One point to be clarified is whether the weak shock wave BB' required to turn the burned gas flow could interfere with the Mach line AA' and thus affect the calculated expansion force on the effusor surface. (Incidentally, if it did, a considerable increase in pressure on the

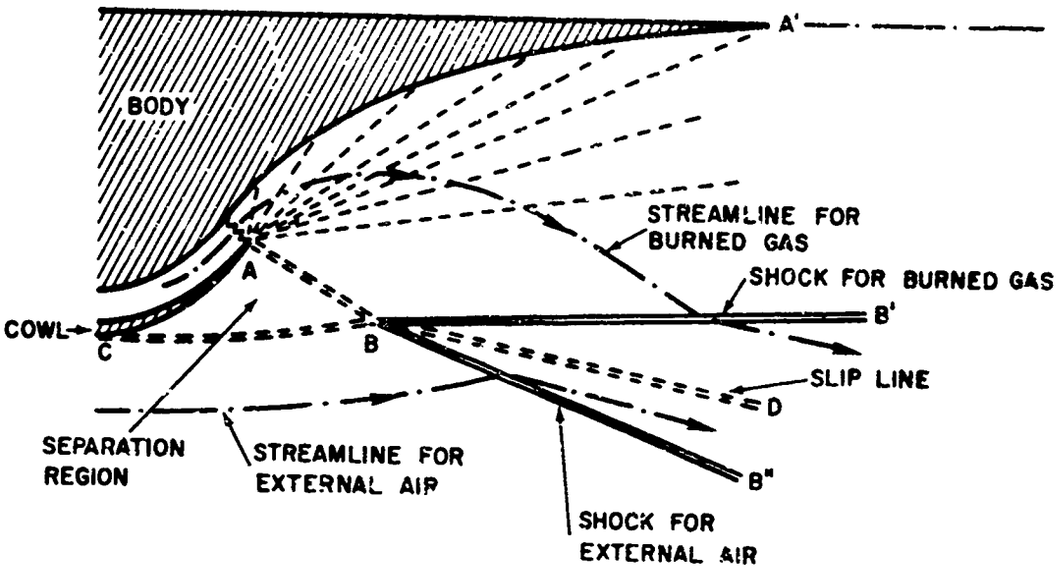

Fig. 26(a) MODEL USED TO EXAMINE VALIDITY OF PRANDTL-MEYER EXPANSION CALCULATIONS: EFFECTS OF FLOW SEPARATION BENEATH COWL

effusor surface would result, compounded to some degree by a flow separation in the effusor boundary layer (see, for example, Ref. 28), so that calculations could only be conservative in this respect.) This possibility was investigated for $P_5/P_O = 5$ and $P_5/P_O = 1$, where P_5 is the pressure at Mach line AA', and the burned gas flow is parallel to the top surface of the engine as it crosses AA'. These pressure ratios bracket the region of greatest interest with respect to providing high I_f L/D. In both cases it was assumed that the pressure along AB was 0.5 P_O and that the external airflow was at Mach 5 and P_O at point C. These assumptions required the external air to be turned through 5.3° (accelerated to Mach 5.62) upon reaching point B and then deflected 16.6° (or 11.3° below the flight axis) by the shock BB''. The shock angle for the external air flow at Mach 5.62 was 25°, and the pressure along BD was 3.23 P_O. For both $P_5/P_O = 5$ and $P_5/P_O = 1$ the shock line BB' and the Mach line AA' were divergent, so that there could be no interference.

If the pressure along AB, P_{AB}, were greater than P_O, then a shock would occur at point C, and the external air flow again would be turned and compressed, and the part of the cowl above the separation region would contribute positively to engine lift. If P_5 were also $\geq P_{AB}$, then BB' and AA' would still diverge. For the unique case $P_5 = P_{AB} = P_O$ and $\theta_5 = 0$, the line CB would be parallel to the flight axis, the separation region and slip line would become a wake at pressure P_O, and there would be no lift on the rear part of the cowl or the effusor.

It is therefore concluded that the present zero-angle-of-attack, $\theta_5 = O$ calculations are valid so long as $P_5 \geq P_{AB}$. At positive angles

of attack, the lift force would be increased (provided that the diffuser efficiency did not drop much), and the thrust force decreased.

The extremely unlikely case of attached external flow was also considered. (For low exit flow angle θ_4 or for positive angles of attack, flow separation could be delayed or prevented by suction on the cowl trailing surface, but in the absence of suction or for flight at an angle of attack less than θ_4, it is quite likely that separation will occur.) If separation does not occur, then in these zero-angle-of-attack calculations the external air flow is accelerated to a very high Mach number by Prandtl-Meyer expansion around the cowl and then deflected by a shock wave AB" to follow the slip plane AD [Fig. 26(b)]. Approximate calculations were attempted for several θ_4's, but no solution was found for a weak shock at AB". A strong shock solution is also impossible for the θ_4's of interest, because the pressure in the subsonic flow region behind the shock would be $< 0.01\ P_O$, and the burned gas flow could not be expanded to such a low pressure before meeting the same shock. The separated flow model is therefore the proper one to use.

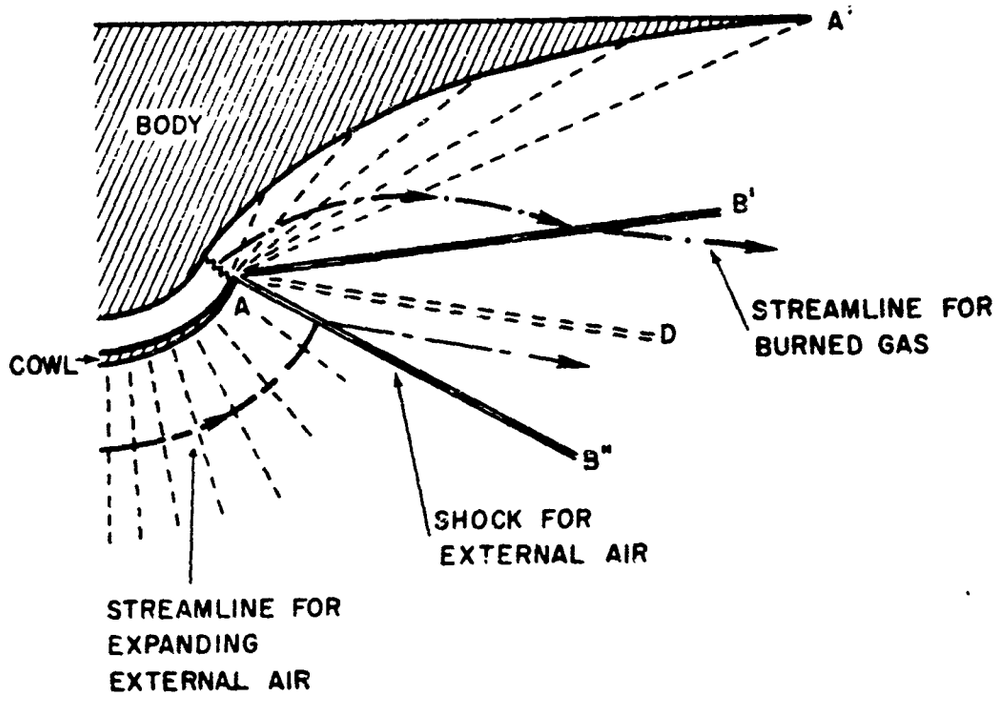

Fig. 26(b) MODEL USED TO EXAMINE VALIDITY OF PRANDTL-MEYER EXPANSION CALCULATIONS; ATTACHED FLOW BENEATH COWL

REFERENCES

1. Perchonok, E., The Hypersonic Ramjet (Confidential) Presented at National Flight Propulsion Meeting, Institute of Aeronautical Sciences, Cleveland, Ohio, ASTIA No. 152267, March 1958.

2. Dugger, G. L., "A Future for Hypersonic Ramjets," Astronautics, Vol. 4, April 1956, pp 38-39, 114-115.

3. Bagnall, E. C. and Zelinski, J. J., Thrust Coefficient and Fuel Specific Impulse for Kerosene-Burning Ramjet at a Flight Mach Number of 10, Applied Physics Laboratory, The Johns Hopkins University, CF-2714, February 1958.

4. Allen, H., Jr. and Fletcher, E. A., Combustion of Various Highly Reactive Fuels in a 3.84- by 10-inch Mach 2 Wind Tunnel, National Aeronautic and Space Agency, Memo 1-15-59E, April 1959.

5. Avery, W. H., "State of the Art, 1961 - Ramjets," Astronautics, Vol. 6, December 1961, p. 48 (see reference to external ramjet studies).

6. Dunlap, R., Brehm, R. L., and Nicholls, J. A., "A Preliminary Study of the Application of Steady-State Detonative Combustion to a Reaction Engine," Jet Propulsion, Vol. 28, July 1958, p. 451.

7. Nicholls, J. A., Dabora, E. K., and Gealer, R. L., "Studies in Connection with Stabilized Gaseous Detonation Waves," Seventh Symposium (International) on Combustion, Butterworth's Scientific Publications, London, 1948, p. 766.

8. Roy, P. M., Propulsion Supersonique par Turboreacteurs et par Statoreacteurs. Paper read at First International Congress in the Aeronautical Sciences under the auspices of the International Council of the Aeronautical Sciences, Madrid, Spain, September 8-13, 1958. (Preprint by Pergamon Press, New York, N. Y.)

9. Gross, R. A., Supersonic Combustion Tunnel (Design Report) Fairchild Engine Division, Deer Park, N. Y., Contract AF 49 (638)-15, October 1957.

10. Rhodes, R. P., Rubins, P. M., and Chriss, D. E., The Effect of Heat Release on the Flow Parameters for Shock-Induced Combustion, Arnold Engineering Development Center, AEDC-TDR-62-78, May 1962.

11. Dorsch, R. G., Serafini, J. S., and Fletcher, E. A., A Preliminary Investigation of Static Pressure Changes Associated with Combustion of Aluminum Borohydride in a Supersonic Wind Tunnel, National Advisory Committee for Aeronautics, RM E55F07, August 1, 1955.

12. Dorsch, R. G., Serafini, J. S., and Fletcher, E. A., Exploratory Investigation of the Aerodynamic Effects of External Combustion of Aluminum Borohydride in Airstream Adjacent to Flat Plate in Mach 2.46 Tunnel, National Advisory Committee for Aeronautics, RM E57E16, 1957.

13. Serafini, J. S., Dorsch, R. G., and Fletcher, E. A., Exploratory Investigation of Static- and Base-Pressure Increases Resulting from Combustion of Aluminum Borohydride Adjacent to Body of Revolution in Supersonic Wind Tunnel, National Advisory Committee for Aeronautics, RM E57E15, October 2, 1957.

14. Dorsch, R. G., Serafini, J. S., Fletcher, E. A., and Pinkel, I. I., Experimental Investigation of Aerodynamic Effects of External Combustion in Air Stream Below Two-Dimensional Supersonic Wing at Mach 2.5 and 3.0, National Aeronautic and Space Agency, Memo 1-11-59E, March 1959.

15. Gazley, Carl, Jr., Linearized Solution for Heat Addition at the Surface of a Supersonic Airfoil, Rand Corporation, RM 1892, ASTIA No. 133025 , 1956.

16. Mager, Artur, "Supersonic Airfoil Performance with Small Heat Addition," Journal of Aeronautical Science, Vol. 26, February 1959, pp. 99-107.

17. Willmarth, W. W., The Production of Aerodynamic Forces by Heat Addition on External Surfaces of Aircraft, Rand Corporation, RM-2708, ASTIA No. 1506 81 , December 1957.

18. Smith, E. H., and Davis, T., The Creation of Thrust and Lift by Combustion on External Surfaces of Airfoils (Confidential), Smith and Davis, Physicists, Silver Spring, Md. (BuOrd Contract NOrd 12141) September 1, 1952.

19. Pinkel, I. I., Serafini, J. S., and Gregg, J. L., Pressure Distribution and Aerodynamic Coefficients Associated with Heat Addition to Supersonic Air Stream Adjacent to Two-Demensional Supersonic Wing, National Advisory Committee for Aeronautics, RM E51K26, 1952.

20. Wald, Q., Reduction of Drag at Supersonic Velocities by Heating the External Air Stream, United Aircraft Corporation, Research Department, M-13362-2, June 5, 1950.

21. Woolard, H. W., An Approximate Analysis of the Two-Dimensional, Supersonic Flow Along a Plane Wall with Supercritical Heat Addition in a Normal Plane, Applied Physics Laboratory, The Johns Hopkins University, CF-2813, March 1959.

22. General Electric Company, Properties of Combustion Gases System: C_nH_{2n} - Air. Volume I. Thermodynamic Properties, McGraw-Hill Book Company, Inc., New York, 1955.

23. Ames Research Staff, Equations, Tables, and Charts for Compressible Flow, National Advisory Committee for Aeronautics, Report No. 1135, 1953.

24. Kennedy, E. C., New Mach Number Tables for Ram-Jet Flow Analysis, $\gamma = 7/5$ and $\gamma = 9/7$, Convair, A Division of General Dynamics Corporation, Ordnance Aerophysics Laboratory, Memo 50-1, August 2, 1955. (Also listed as CF-1798-A.)

25. Liepmann, H. W. and Puckett, A. E., Introduction to Aerodynamics of a Compressible Fluid, John Wiley and Sons, Inc., New York, N. Y., 1947.

26. Eggers, A. J., Jr., Allen, H. J., and Neice, S. E., A Comparative Analysis of the Performance of Long Range Hypervelocity Vehicles, National Advisory Committee for Aeronautics, TN 4068, October 1957.

27. Hoerner, S. F., Fluid--Dynamic Drag. (Published by the author), 1958.

28. Kuethe, A. M. and Shetzer, J. D., Foundations of Aerodynamics, John Wiley and Sons, Inc., New York, 1950, p. 305.

ACKNOWLEDGMENT

The feasibility study of external ramjets was supported by the Bureau of Ordnance, Department of the Navy, under Contract NOrd-7386. In 1962 this contract was changed to NOw 62-0604-c, supported by the Bureau of Naval Weapons, Department of the Navy. The authors are particularly grateful for the encouragement, advice, and support of Mr. Frank I. Tanczos. Technical contributions by and helpful discussions with various members of the Applied Physics Laboratory are gratefully acknowledged, with particular notice to the following: Dr. W. H. Avery; Mr. J. L. Keirsey, who first suggested the model of Fig. 6; Mr. H. D. Black, who assisted with Section IV; Messrs. R. H. Cramer and J. H. Walker for permission to use and help in preparation of Section V; and Mrs. E. Bagnall, who did many of the computations.

UNCLASSIFIED

Security Classification

DOCUMENT CONTROL DATA – R&D

(Security classification of title, body of abstract and indexing annotation must be entered when the overall report is classified)

1. ORIGINATING ACTIVITY (Corporate author)	2a. REPORT SECURITY CLASSIFICATION
The Johns Hopkins Univ., Applied Physics Lab. 8621 Georgia Avenue Silver Spring, Maryland	Unclassified
	2b. GROUP

3. REPORT TITLE

External Burning Ramjets Preliminary Feasibility Study

4. DESCRIPTIVE NOTES (Type of report and inclusive dates)

Technical Memorandum

5. AUTHOR(S) (Last name, first name, initial)

Dugger, G. L. and Monchick, L.

6. REPORT DATE	7a. TOTAL NO. OF PAGES	7b. NO. OF REFS
March 1967	89	28

8a. CONTRACT OR GRANT NO.	9a. ORIGINATOR'S REPORT NUMBER(S)
NOw 62-0604-c b. PROJECT NO. Task Assignment A55 c. d.	TG-892 9b. OTHER REPORT NO(S) (Any other numbers that may be assigned this report)

10. AVAILABILITY/LIMITATION NOTICES

Distribution of this document is unlimited.

11. SUPPLEMENTARY NOTES	12. SPONSORING MILITARY ACTIVITY
	Naval Ordnance Systems Command Department of the Navy

13. ABSTRACT

Experiments and analyses at the Applied Physics Laboratory and elsewhere have shown that burning beneath external surfaces of a supersonic vehicle can produce lift and reduce drag. Preliminary analyses of some two-dimensional external burning ramjet (ERJ) and external expansion ramjet (EERJ) models yield some encouraging results. The EERJ uses ducted subsonic combustion but all-external expansion, so that the two-dimensional (or half-round) nozzle obtains some heat relief by radiation and contributes to vehicle lift, increasing lift/drag ratio. Effects of vectoring the EERJ nozzle and advantages and disadvantages of substituting a simple ramp in place of the nonreflecting surface are explored briefly. Three possible paths for the design of hypersonic transport vehicles incorporating EERJ's for cruise power and auxiliary lower speed engines are pictured and discussed in general terms.

DD FORM 1 JAN 64 1473

UNCLASSIFIED

Security Classification

14. KEY WORDS

Ramjet Propulsion Systems
Ramjets - Cooling
Ramjets - Thrust